JOURNAL
OF
GEOMAGNETISM
AND
GEOELECTRICITY

VOL. IX NO. 1

SOCIETY
OF
TERRESTRIAL MAGNETISM AND ELECTRICITY
OF
JAPAN

MARCH 1957
KYOTO

JOURNAL OF GEOMAGNETISM AND GEOELECTRICITY

EDITORIAL COMMITTEE

EDITORIAL OFFICE: Society of Terrestrial Magnetism and Electricity of Japan, Geophysical Institute, Kyoto University, Kyoto, Japan

The fields of interest of this quarterly Journal are as follows:

Terrestrial Magnetism	Aurora and Night Airglow
Atmospheric Electricity	The Ozone Layer
The Ionosphere	Physical States of the Upper Atmosphere
Radio Wave Propagation	Solar Phenomena relating to the Above Subjects
Cosmic Rays	Electricity within the Earth

The text should be written in English, German or French. The price is set as 1 dollar per number. We hope to exchange this Journal with periodical publications of any kind in the field of natural science.

The Editors

Disturbances in the Ionospheric $F2$ Region Associated with Geomagnetic Storms II. Middle Latitudes

By Teruo SATO

Geophysical Institute, Kyoto University

(Read Oct. 17 1956; Received, Mar. 1 1957)

Abstract

An attempt is made to account for the $F2$ disturbances in middle latitudes associated with the geomagnetic storms in term of the vertical drift of the electron. For this purpose, at first it is shown that in middle latitudes the variations of $foF2$ on the storm day are classified in two types, negative and positive disturbances, the former of which is the same as the representative variation in high latitudes while the latter the analogous to the variation in low latitudes (including the equator), on the other hand, the variations of $h'F2$ are analogous to those in high and low latitudes, regardless of the seasons.

The vertical drift of the electron is considered to be caused by an electric field deduced from the disturbance-daily variation of the geomagnetic field. The results of the calculations for individual states show that two types of disturbances in middle latitudes seem to be explained as an effect of the vertical drift of the electron, though the coincidence between the observed and calculated for the positive type is not sufficient. From the above results, together with the results previously obtained for the equatorial zone, it is found that the occurrence of the positive or negative disturbances is ascribed to the conditions that the phase of the drift velocity of the electron on the quiet day is the same as that of the drift velocity on the disturbed day (negative) or the phase of the former differs from that of the latter by about 180° (positive). It is also found that the seasonal and latitudinal variations of the $F2$ disturbance are due to the existence of the S_q dynamo current in the ionosphere.

1. Introduction

The ionospheric $F2$ disturbances associated with geomagnetic storms have been studied theoretically by several authors. The theories are divided generally into three kinds. The first of them is the thermal expansion theory [1], [2], the second is the electron drift theory [3], [4] and the third is the recombination theory [5]. Of these theories, the electron drift theory is considered to be the most suitable one, because the ionospheric disturbances have the following characteristics:

(a) The disturbances in the $F2$ regin are caused almost simultaneously in many stations of the world.

(b) When the disturbance begins in the $F2$ region, disturbances begin simultaneously in the $F1$ and even in the E regions [6]. The daily variations and the seasonal or

latitudinal changes of the deviations from the normal of the critical frequencies of the $F1$ and E regions are significantly analogous to those in the $F2$ region. [7].

Based on the above characteristics, the explanation of the $F2$ disturbances in middle latitudes is at first attempted for an average state of the disturbances by the drift theory by the author [8]. The results of the study show that the effects of the electron drift are very important. However, it seems to be better to study the $F2$ disturbances for their individual state, because they are fairly different from the averge state. From this point of view, the drift theory is also apllied by the author to the study of the individual $F2$ disturbances in the equatorial zone, using the data at Huancayo. The results reveal that the individual $F2$ disturbances in the equatorial zone are well explained as the effect of the vertical drift of the electron [9].

In this paper it is attempted to explain the individual $F2$ disturbances in middle latitudes by the electron drift theory and furthermore, based on the results of the calculations for the $F2$ disturbances in middle latitudes and in the equatorial zone, the features of the variations of the $F2$ disturbances with latitude, season, and sunspot or geomagnetic activities are physically explained. For these purposes individual $F2$ disturbances are classified into two kinds and the features of their seasonal or latitudinal occurrences are stitistically clarified.

2. Some Statistical Results of $F2$ disturbances

Statistical studies of the $F2$ disturbances are carried out by many authors [1], [3], [10]–[16] and the storm time deviations of the $foF2$ and $h'F2$ (critical frequency and virtual height of the $F2$ region) and their variations with season, latitude, and sunspot or geomagnetic activities are discussed. However, as the $F2$ disturbances in middle latitudes are complicated compared with those in other latitudes, the results derived somtimes seem to differ depending on the period, the year of the data and the number of the geomagnetic storms used there. This is because in many studies the attention is not paid for the type of the $F2$ disturbances. For this reason it is better to classify the daily variation of the deriation of the $F2$ disturbance by a suitable method and take statistics of the respective types of the disturbances. Up to the present time, the classification of the $F2$ disturbances has been attempted by some authors [10], [11], but theoretical bases of them are ambiguous. In this section we attempt a classification of the $F2$ disturbances and make their features clear.

Glancing over many disturbances over the world, it is found that the daily variation of f_0F2 is classified into the following two types:

(1) The f_0F2 decreases from the normal in daytime with a maximum depression about at noon and recovers to the normal value or rather increases at night.

(2) The $foF2$ tends to increase in daytime or/and at night. Sometimes $foF2$ decreases early in the morning.

In an actual case, one of the above variations is superposed on the other. We call tentatively the type (1) the 'negative disturbance'and the type (2) the 'positive disturbance' (compare with Appleton and Piggot [11]). These two types of the $F2$ disturb-

ances are basic types, independently of the height variation (it is known in the follwing that the height deviations are always the same in every latitudes) and the physical meaning of the occurence of them is shown in the section 7. The mean daily variations of the deviations (Δf_0F2) in two types are shown in Fig. 1 for five stations, College (geographic latit. 64.°9, geomagnetic latit. 64.°5) Washington (39.°0, 50.°0), Watheroo (−30.°19,−41.°8), Kokubunji (35.°7, 26.°0), and Huancayo (−12.°03,−0.°6). The blanks in Fig. 1 show rarity of the occurrence of the positive disturbance in high latitudes and negative disturbance in low latitudes or in the equator.

Next we treat the $h'F2$ variation on the storm day. We should pay an attention to the derivation of the deviation of $h'F2$, because of the inclusion of the retardation effect of the radio wave through the $F1$ region. Especially, in the case of the negative disturbance this effect is very great. The evidences are shown in Fig. 2 and A and D in Fig. 6. Since the $foF2$ becomes very low due to the disturbance, the difference between f_0F2 and f_0F1 (critical frequeney of the $F1$ region) becomes very small. Then the deviation of $h'F2$ becoms large abruptly, sometimes it reaches to infinity. When the f_0F2 is far greater than the f_0F1 the deviation of the height is very small and rather the height decreases from the normal value. The retardation effect is absent at night, sets up suddenly at sunrise and disappears gradually as the sunset approaches. This effect is included not only in the $h'F2$,

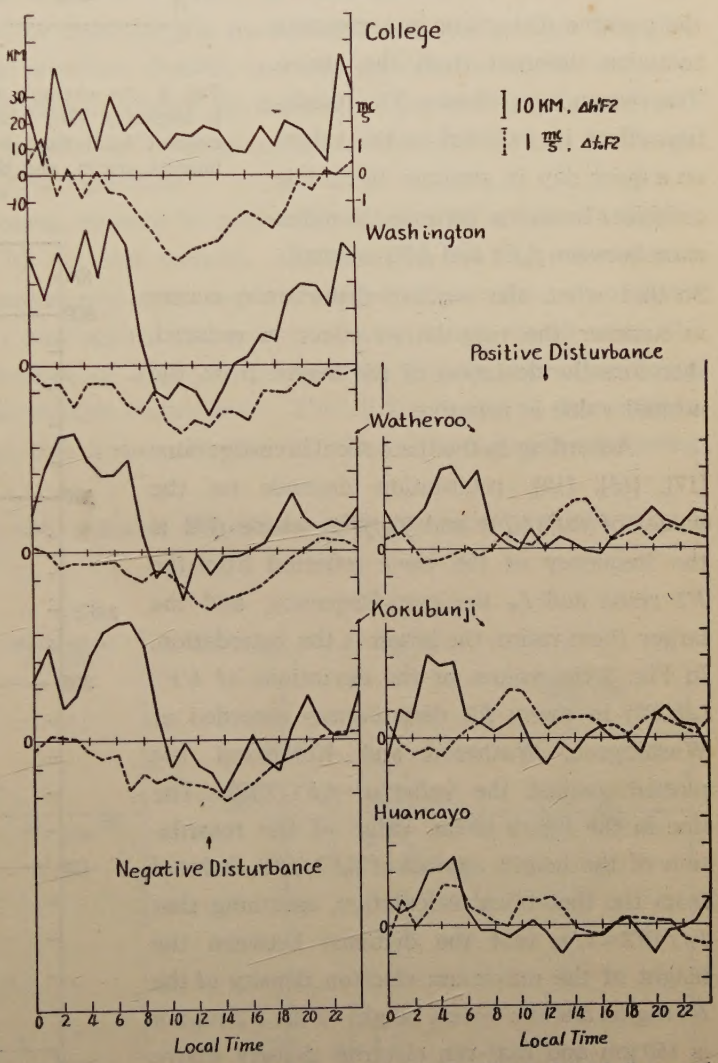

Fig. 1 Observed mean daily variations of $\Delta foF2$ dotted line and $\Delta h'F2$ (deviative values from the normal of $foF2$ and $h'F2$) in the negative and positive disturbances for five stations. The variation is the mean of the remarkable deviations during the years Oct. 1956–Jan. 1957 for College, 1949–1956 for Washington, 1938–1944 for Wetheroo, 1949–1956 for Kokubunji and 1938–1944 for Huancayo.

but also in the h_pF2 (height of the maximum electron density of the $F2$ region), because the latter is deduced from the calculation as to the one parabolic region and the effect of the other region is not taken into account.

We must sometimes pay an attention to the retardation effect in the positive disturbanc in a meaning somwhat different from the above. The reason is as follows. The retadation effect is included in the height on a quiet day in summer in middle or higher latitudes, because the difference between f_0F2 and f_0F1 is small. So that when the positive disturbance occurs in summer the retardation effect is reduced, therefore the deviation of the height from the normal value is negative.

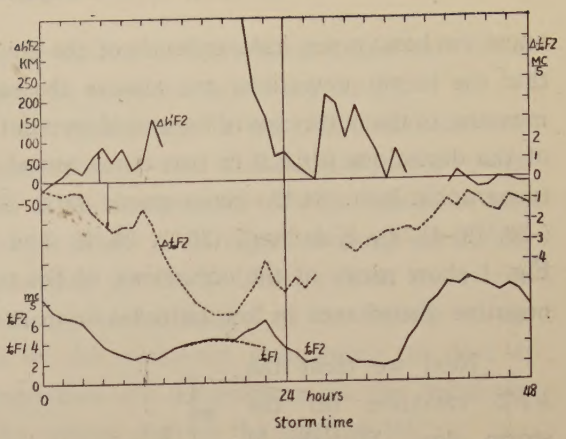

Fig. 2 An example of the $F2$ negative disturbance. It begins at 19h, March 2, 1956. The time is the nearest local time before the beginning of the geomanetic storm, and this time is taken as zero of the storm time.

According to the theoretical investigations [17], [18], [19], retardation depends on the values of $foF1/fF2$ and $f_H/fF2$, where $fF2$ is the frequency of the wave reflected from the $F2$ rgion and f_H the gyro-frequency, and the larger these ratios, the larger is the retardation. In Fig. 3 the values of the deviations of $h'F2$ ($\Delta h'F2$) in many $F2$ disturbances recorded at Washington, Watheroo and Kokubunji are plotted against the value of f_0F1/f_0F2. The line in the figure is the value of the retardation of the height against of $f_0F1/fF2$, deduced from the theoretical calculation, assuming that $f_H/fF2=1/4$, that the distance between the height of the maximum electron density of the $F1$ region and the lowest height of the $F2$ region is 150 km and that the electron density above the maximum density of the $F1$ region is the same as the maximum density of the $F1$ region. Comparing the theoretical values with the observed ones, the coincidence is good for the large values of $foF1/foF2$ and it is not good for the

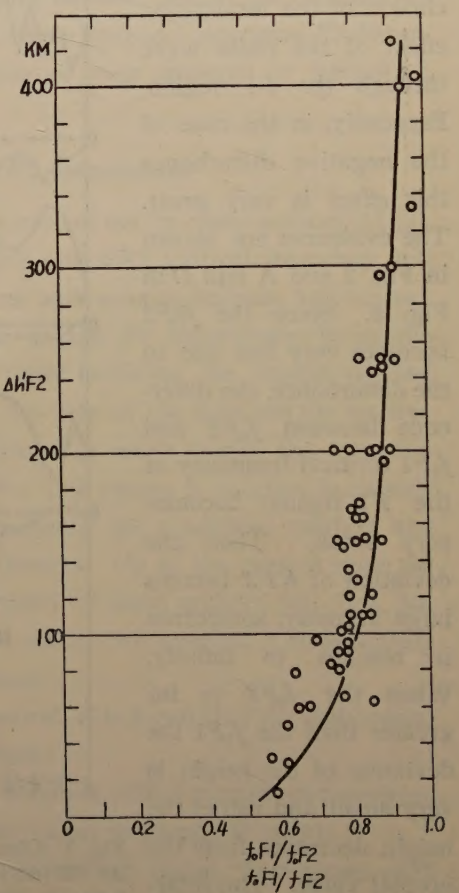

Fig. 3 The magnitude of $\Delta h'F2$ against the value of $foF1/foF2$. The full line in the figure represents the calculated value against the value of $foF1/fF2$ where $fF2$ is the frequency of the radio wave by which the virtual height is measured.

smaller values of it. This is because that $f_0F2 \simeq fF2$ for $f_0F1/f_0F2 \simeq 1$ and $f_0F2 > fF2$ for the lower value of f_0F1/f_0F2, if in the present case we assume that the $f\ F2$ represents the frequency by which the virtual height is measured.

In Fig. 1 the mean daily variations of the deviative values ($\Delta h'F2$) of the height are shown for five stations, after a correction for the retardation is made using the theoretical value shown in Fig. 3. Correction is made mainly for the negative disturbance. As it is difficult to correct the data at College for the lack of f_0F1, the height deviations during Oct. 1956-Jan. 1957, whence the difference between f_0F1 and f_0F2 is considered to be large, are taken. From Fig. 1 it is found that the daily variation of the deviative value of the height is almost the same for the stations from equator to high latitudes, regardless of the type of the variation of *foF2*, and that the features of the variation are the increase at night and small decrease in daytime. Since the height variation is independent of the type of the f_0F2 variation, the classification of the $F2$ disturbances is done only for the f_0F2 variations.

The variations with season, sunspot or geomagnetic activities of the $F2$ disturbances are shown in Fig. 4 for the four stations. In this figure the daily mean values ($\overline{\Delta f_0F2}$) of Δf_0F2 on the first and second storm days are plotted against the sum of three hourly K_p indices of the day and against the sunspot number in the month when the storm occurs. The negative value of $\overline{\Delta f_0F2}$ corresponds to the negative disturbance and the positive value to the positive disturbance. The circles represent the summer, filled circles the winter and the crosses the equinox. From the figure the following points are recognized.

(1) In high latitudes the negative disturbance seems to occur predominantly in three seasons.

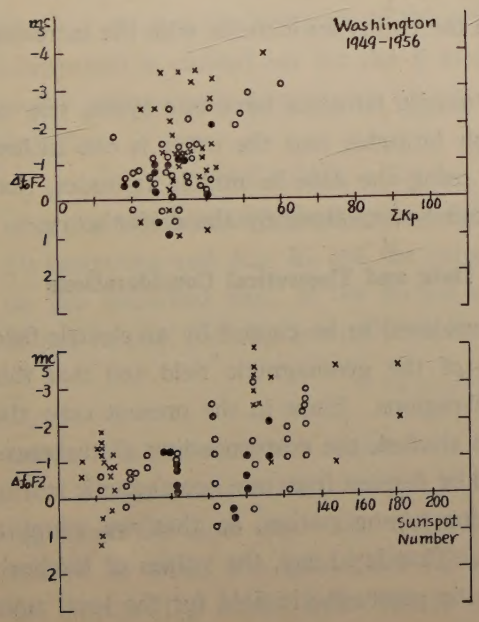

Fig. 4, (a)

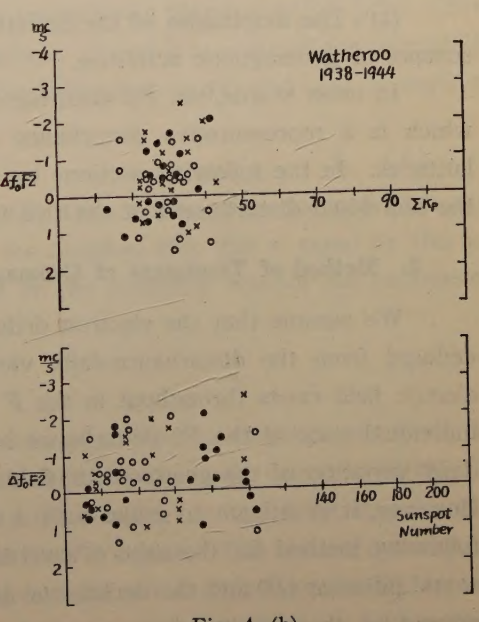

Fig. 4, (b)

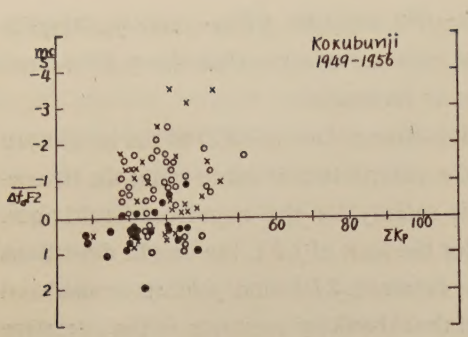

Fig. 4, (c)

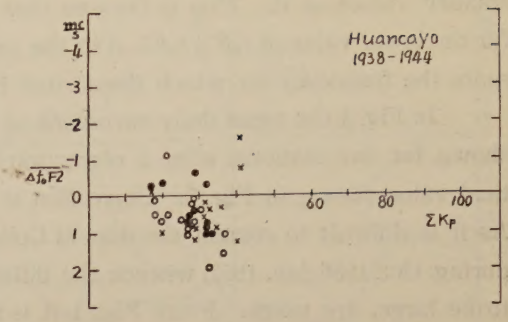

Fig. 4, (d)

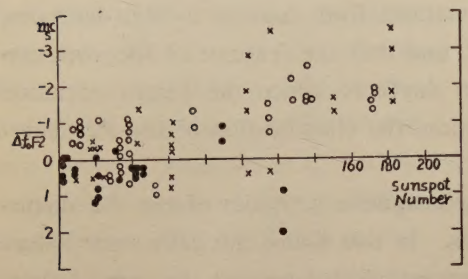

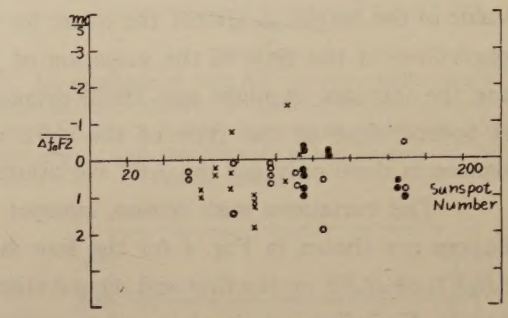

Eig. 4 (a)–(d) The Distribution of $\overline{\Delta f_0 F2}$ (daily mean of $\Delta f_0 F2$) against ΣK_p and against the sunspot number in the month when the disturbance occurs.

(2) In middle latitudes the negative disutrbance seems to occur predominantly in summer or equinox and positive disturbance in winter. For the small sumspot or geomagnetic activities the positive disturbance tends to occur.

(3) In low latitudes or in the equatorial zone the positive disturbance occurs predominantly in three seasons.

(4) The amplitudes of the deviations in the two types increase with the incresing sunspot or geomagnetic activities.

In other words, the $F2$ disturbances in middle latitudes have two types, one of which is a representative disturbance in high latitudes and the other is one in low latitudes. In the following sections we show, using the data in middle latitudes, that the individual disturbances of the two types can be explained by the drift theory.

3. Method of Treatment of Geomagnetic Data and Theoretical Considerations

We assume that the electron drift is considered to be caused by an electric field deduced from the disturbance-daily variation of the geomagnetic field and that this electric field exists throughout in the F and E regions. Since in the present case the individual state of the $F2$ disturbance is to be studied, the corresponding disturbence-daily variation of the geomagnetic field should be derived from one geomagnetic storm. However, it is difficult to make such a deduction in one station, so that we adopt a following method for the sake of convenience. That is to say, the values of the horizontal intensity (H) and the declination (D) of the geomagnetic field for the local time nearest to that of the commencement of the geomagnetic storm, are taken and from

these values the mean values of H and D on the five international quiet days corresponding to that hour are respectively subtracted. The values thus obtained are the deviative parts at hour zero of the storm time. The process is followed for succeeding 60 hours (2 days and 12 hours). They are denoted respectively as ΔH and ΔD. Next the overlapped mean of 24 hours of them are calculated for the former 48 hours, assuming that the deviative values before the commencement of the geomagnetic storm are zero. Then the variations can be said to correspond to the Dst variation of the average state. When these variations are subtracted respectively from ΔH and ΔD, the parts corresponding to the Ds variations of the average state can be derived. They are the requested disturbance-daily variations of the geomagnetic field.

When the disturbance-daily variation Ds is derived, the electric field and then the velocity of the electron drift can be derived, knowing the electrical conductivity of the ionosphere. When an anisotropic electrical conductivity is taken into account and it is assumed that the winds in the E and F regions have the same directions and magnitudes and that the geomagnetic field is produced by the dipole field, the vertical velocity of the electron in the F region is given by [20]

$$v=\left\{\frac{I_x}{K_{xy}}+\frac{I_y}{K_y}\right\}\frac{\sin\theta}{F(1+3\cos^2\theta)^{1/2}} \tag{1}$$

where I_x and I_y represent the total electric currents respectively in the x (south) and y (east) directions flowing in the E and F regions, θ the geomagoetic co-latitude of the station, F the total intensity of the geomagnetic field and

$$K_{xy}=\frac{\Delta}{k_{xy}},\quad K_y=\frac{\Delta}{k_x},\quad \Delta=k_{xy}^2+k_xk_y, \tag{2}$$

where

$$k_x=\int_E\sigma'_{xx}\,dz+\int_F\sigma'_{xx}\,dz,\qquad \text{etc.,} \tag{3}$$

and $\sigma_{xx'}$ etc. are the elements of the electrical conductivity tensor $\sigma'=\begin{Bmatrix}\sigma'_{xx} & \sigma'_{xy}\\ \sigma'_{yx} & \sigma'_{yy}\end{Bmatrix}$. The integration is carried out for the E and F regions. I_x and I_y are related approximately to the geomagnetic components in y and x directions, that is ΔY and ΔX, in such a way that

$$2\pi I_x=f\Delta Y,\qquad 2\pi I_y=-f\Delta X, \tag{4}$$

where f is constant and taken as unity. *If* ΔX, ΔY are the values deduced from the Ds variations and K_{xy}, K_y are the values on the distubed day, the v equal to the v_d on the disturbed day. If the station situates on the magnetic equator the expression of the vertical velocity is simplified as follows,

$$v=\frac{\Delta X}{2\pi KF} \tag{5}$$

where K is the electrical conductivity of the ionosphere on the magnetic equator.

In the course of the study it is necessary to know the daily variation of the $F2$ region on the quiet day. The vertical drift of the electron on the quiet day is considered to affect the quiet daily variation of the $F2$ region. The vertical velocity of the electron (v_q) on the quiet day is obtained by the same expression as (1) or (5), replacing the electrical conductivity and the variations of the geomognetic field in their

expressions by the values on the quiet day. The values of ΔX and ΔY are those derived from the mean value of the S_q variations of the five international quiet days in the month when the storm occurs.

If the effect of the horizontal velocity and the height-gradient of the vertical velocity are not taken into account, the variation of the electron density is given by

$$\frac{\partial n}{\partial t}=q\,(t,z)-\beta\,(z)-v(t)\frac{\partial n}{\partial z} \qquad (6)$$

where n represents the electron density, v the vertical velocity of the electron, q and β the production and effective attachment rates of the electron respectively, t the time and z the height in the unit of the scale height. q is taken as $q_0 exp\ (1-z-e^{-z}\ \sec\chi)$, where q_0 is constant and χ is the solar zenith distance. The height distribution of β used for calculations is shown in Fig. 5. The equation (6) is solved by the numerical method firstly attempted by Millington [21]. Then the equation is replaced by the following forms

$$\sigma_0\frac{d\nu}{d\phi}=|F|_z-|\xi|_z\nu \qquad (7)$$

$$\frac{dz}{d\phi}=1.37\times10^4 v$$

where $t=1.37\times10^4\phi$, $1/\sigma_0=1.37\times10^4\beta_0$, $1/n_0=\beta_0/q_0$, $\nu=n/n_0$, $\beta=\beta_0|\xi|_z$ (β_0 is constant) and $|F|_z=exp(1-z-e^{-z}\ \sec\chi)$. If the velocity v equals to v_q the solution of the equation represents the daily variation on the quiet day and if v equals to v_q+v_d the solution represents the daily variation on the disturbed day. When the former variation is subtracted from the latter the residuum equals to the deviation from the normal variation.

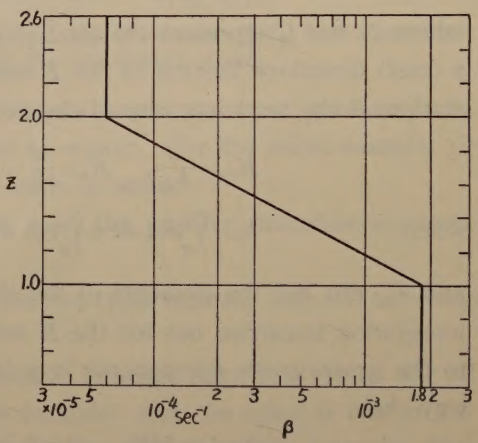

Fig. 5 Height-distribution of β.

4. *F*2 Negative Disturbances

In sections 4 and 5 the $F2$ disturbances in middle latitudes are studied for their individual states. The ionospheric data are those at Washington, during the years 1949–1952, Watheroo, 1939–1944, and Kokubunji 1949–1955 and the corresponding geomagnenic data are those at Cheltenham (geographic latit. 38.°44, geomagnetic latit. 50.°1), Watheroo and Kakioka (36.°14, 26.°0) for the same periods respectively.

The calculations of the deviative values of the maximum electron density and the height are made and they are compared with the corresponding variations of the ionospoeric data. The daily variation of the electrical conductivity is taken such as

$$K_{xy}=1.6\times10^{-8}\ p(t),\ e.m.u \qquad (8)$$
$$K_y=3.0\times10^{-8}p(t),\ e.m.u$$

Table 1 $p(t)$ on the quiet day

local time	0^h	2	4	6	8	10	12	14	16	18	20	22
summer	0.48	0.42	0.42	1.2	2.4	4.0	4.6	4.0	2.4	1.5	1.0	0.6
equinox	0.43	0.41	0.41	1.1	2.2	3.6	4.2	3.6	2.2	1.2	0.8	0.5
winter	0.40	0.35	0.35	1.0	2.0	3.3	3.8	3.3	2.0	1.0	0.6	0.5

Table 2 $p(t)$ on the disturbed day

local time	0^h	2	4	6	8	10	12	14	16	18	20	22
summer	3.0	3.0	3.2	3.2	3.6	4.0	4.6	4.0	3.6	3.2	3.2	3.0
equinox	2.7	2.7	3.0	3.0	3.2	3.6	4.2	3.6	3.2	3.0	3.0	2.7
winter	2.5	2.5	2.7	2.7	2.9	3.3	3.8	3.3	2.9	2.9	2.7	2.5

for three stations for the sake of simplicity. The daily variation factor $p(t)$ varies with season. It is shown in Table 1 for the quiet day and in Table 2 for the disturbed day.

In Table 2 we assume that the electrical cunductivity at night is comparable order of magnitude with that in daytime, though it is doubtful whether the assumption is correct or not. This assumption is derived from the fact that the geomagnetic variation on the disturbed day at night is equivalent to that in daytime.

The method of the calculation of the deviative variations is stated in the section **3.** The results for some ionospheric disturbaces are shown in Fig. 6 (a)–(n). In these figures the part A represents the observed variations of $\Delta foF2$ and $\Delta h'F2$ (or $\Delta h_F F2$), B, the corresponding calculated values, C, the disturbance-daily variations of ΔH and

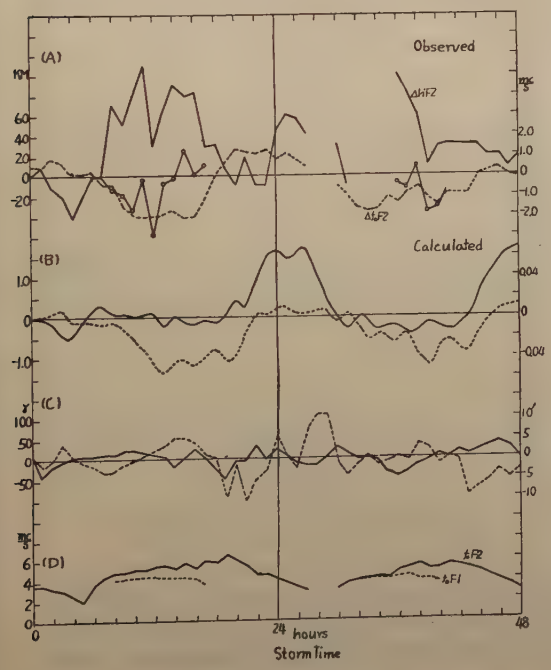

(a) Washington, 0^h, Sep. 7, 1952

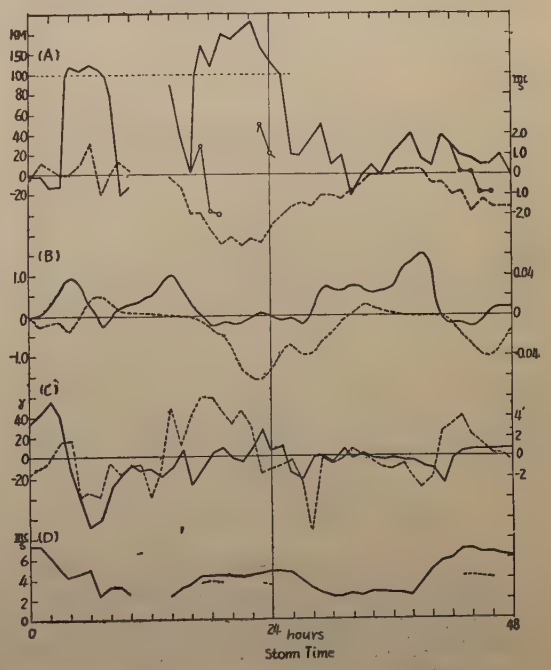

(b) Washington, 16^h, Feb. 23, 1952

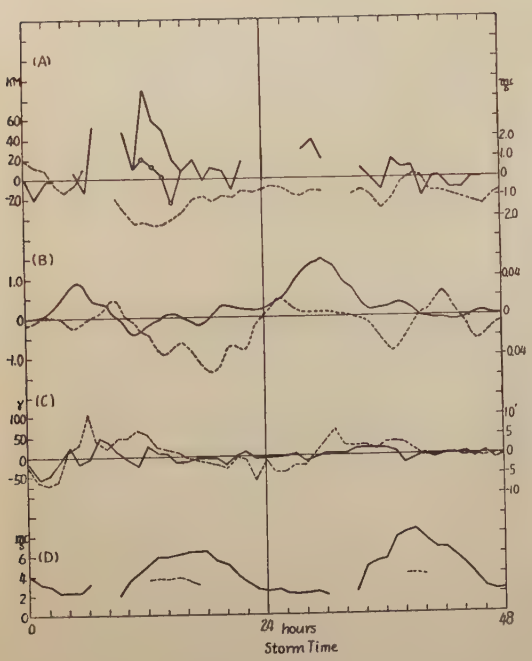

(c) Washington, 22^h, Jan. 4, 1952

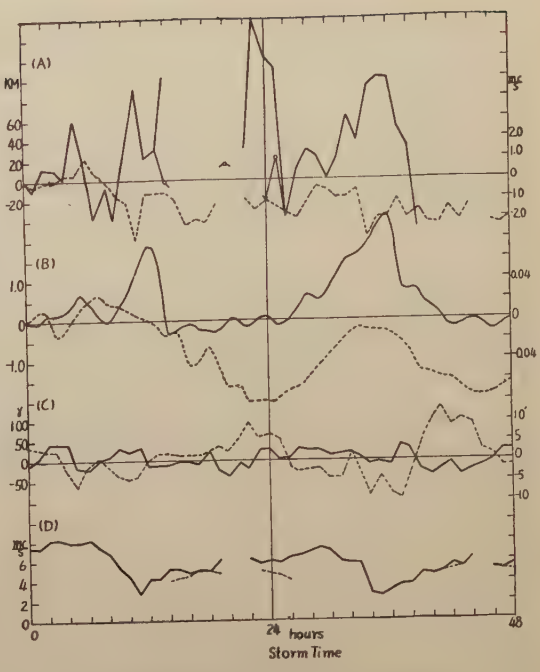

(d) Washington, 16^h, Jun. 3, 1949

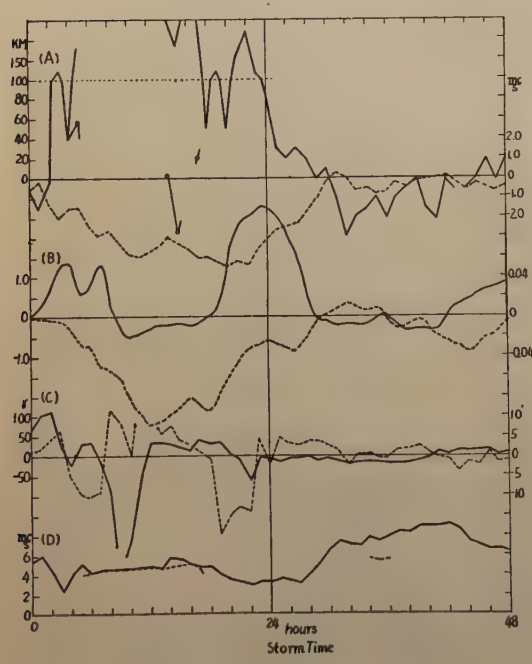

(e) Washington, 1^h, May 12, 1949

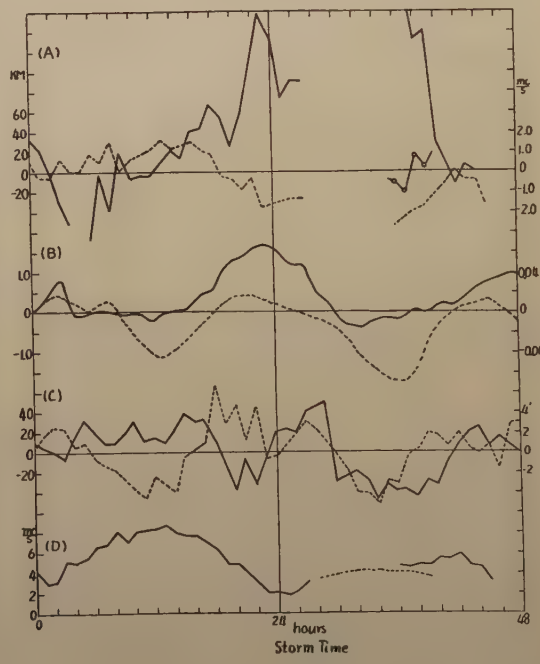

(f) Watheroo, 3^h, Dec. 16, 1944

Fig. 6, (a)–(n) Observed and calculated deviations of individual negative disturbance. (A) represents the observed variations of Δf_0F2 (dotted line, right ordinate), $\Delta h'F2$ (or $\Delta hpF2$ for kokubunji, full line, left ordinate) and the *corrected variation* of $\Delta h'F2$ (*full line with circle*) for the $F2$ disturbance which begins at the time shown below. The time is the nearest local time before the beginning of the geomagnetic storm and this time is taken as zero of the

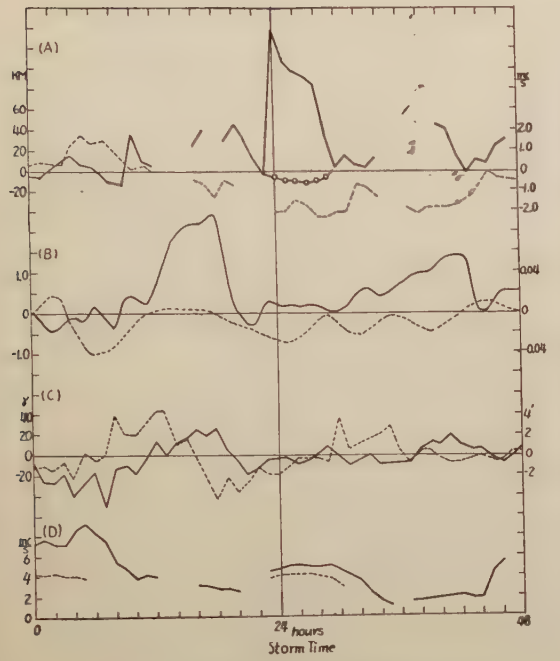

(g) Watheroo, 10^h, May 1, 1943

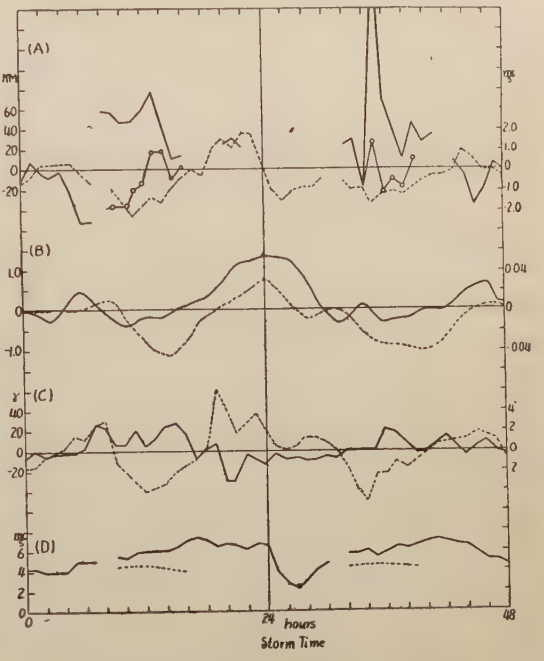

(h) Watherffo, 1^h, Dec. 21, 1942

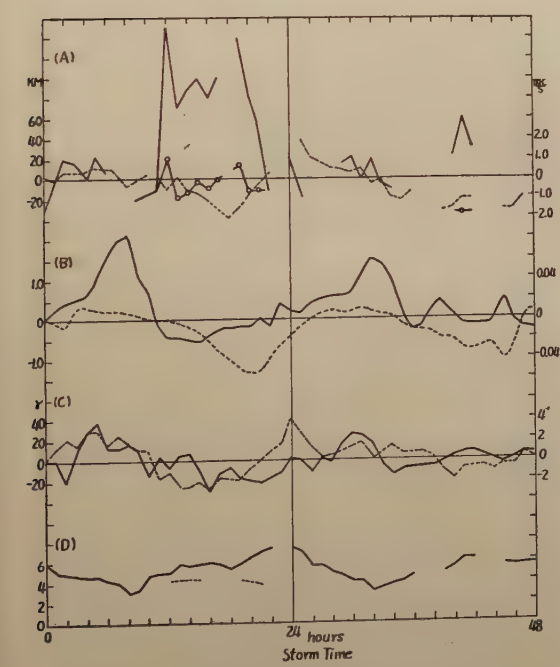

(i) Watheroo, 20^h, Nov.23, 1942

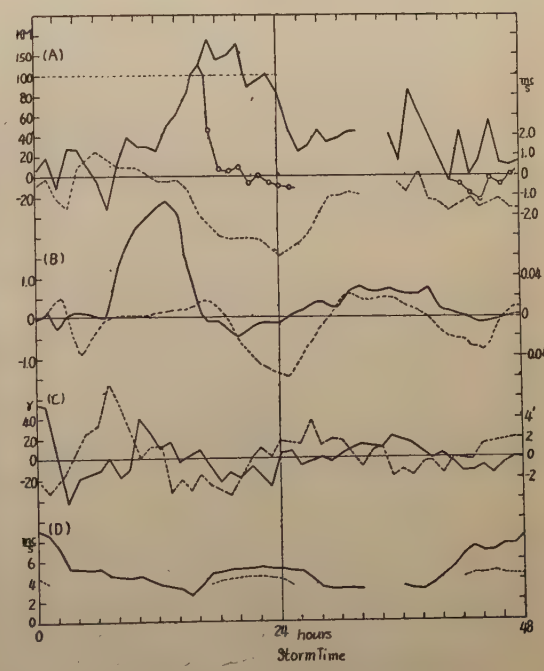

(j) Watheroo, 15^h, Apr. 24, 1941

storm time. (B) represents the calculated variations of the deviations of the maximum electron density (dotted line, right ordinate) and the height (full line), (C) the observed geomagnetic disturbance-daily variatons of ΔH (full line, left ordinate) and ΔD (dotted line) and (D) the $foF2$ and $foF1$.

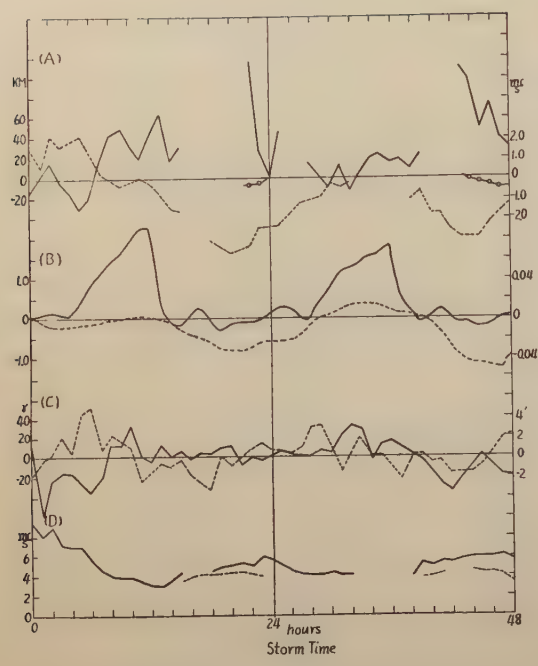

(k) Watheroo, 17^h, Mar. 28, 1941

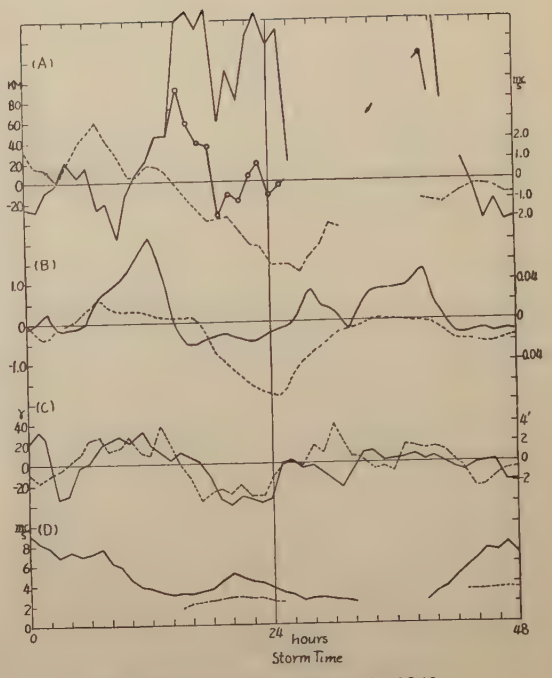

(l) Wathroo, 15^h, Nov. 12, 1940

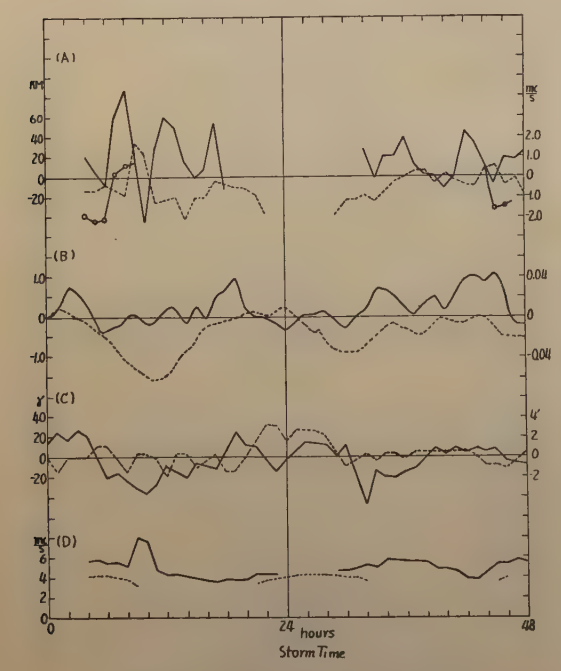

(m) Kokubunji, 9^h, Jul. 5, 1952

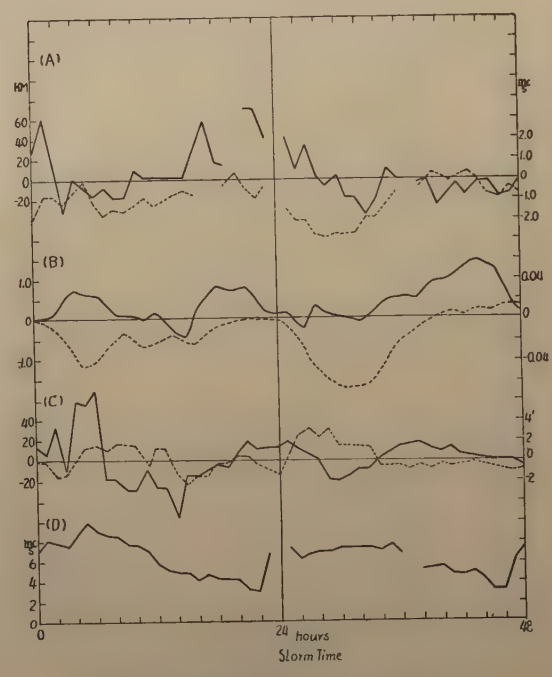

(n) Kokubunji, 7^h, Sep. 12, 1949

ΔD of the geomagnetic field, and D the values of $foF2$ and $foF1$. As mentioned above, the characteristic of the negative disturbance is the remarkable depression of $foF2$ in daytime. The results of the calculations show this tendency, but the time of the maximum depression seems to lag one or two hours. Also the increase of f_0F2 in

some examples are not obtained in our calculations.

As shown in the section **2**, it is evident that the large increase of the height in daytime is considered to be the retardation of the radio wave, so that the correction should be made for these values. The correction in Fig. 6 is made based on the theoretical curve shown in Fig. 3 and the corrected variations are shown by a full line with circle. Then it is clear that the calculated variations of the height are consistent with the corrected variations.

Conclusively it can be said that the $F2$ negative disturbances are well explained by the drift theory.

5. $F2$ Positive Disturbances

At first we must take care of the fact that two types of apparent positive disturbance may take place. One is a type where the fluctuation of the solar radiation responsible for formation of the $F2$ region leads to the apparent positive deviation. The other is a type seen when many days of the negative disturbance exist in a month, for the normal variation is mistaken as a positive disturbance, since the median value of the month becomes lower than the normal value. In the following the above apparent disturbances are excluded.

Now, calculations of the deviations of the maximum electron density and the height for some positive disturbances are carried out by the same process as those for the negative disturbance. The stations and periods of the data used are the same as those in the negative disturbance, and the electrical conductivities are those shown in (8). The results are shown in Fig. 7 (a)–(d). In these figures the parts A to C correspond to those in Fig. 6. From figure 7 it is found that the calculated variation of the height accords well with the observed, while the calculated variation of the electron density does not show sufficient coincidence, though the accordance seems to be good for the first day.

It is important to know that the increase of the electron density is caused by the vertical drift of the electron. This is, as shown in the section **7**, due to the mechanism that the drift velocity on the quiet day is reduced by the drift velocity additively generated on the disturbed day, so that the region tends to cease to move (the electron density on the static region is larger than that of the moving region). The insufficient coincidence in Fig. 7 is perhaps due to the fact that the daily variation of the drift velocity deduced from the S_q variation on the quiet day is somewhat different from the actual state in the $F2$ region and the machanism of the increment does not become effective. The phase and the magnitude of the drift velocity depend on the values of K_{xy} and K_y, and are modified by the induced field by the wind in the $F2$ region. Especially, the effect of the wind in the $F2$ region may give rise to the different phase or magnitude of the electric field in that region from those in the E region. (This possibility is larger in winter than in summer, since the electron density in the former season is larger than that in the latter [29], [30].) We must also pay an attention to the fact that the wind from the observation in winter varies diurnally, while the

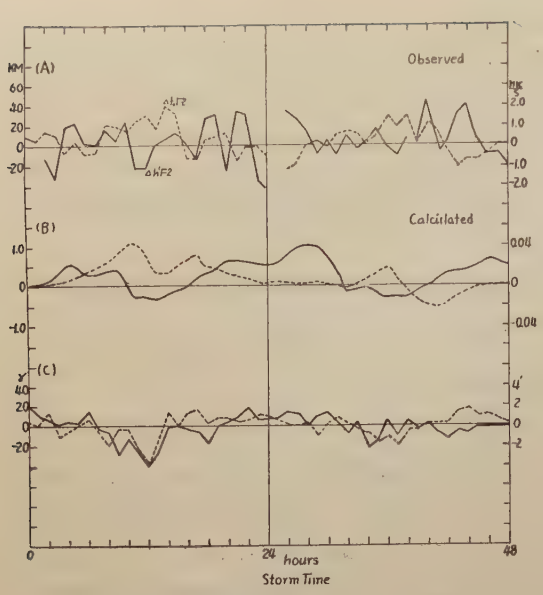

(a) Watheroo, 1^h, May 18, 1943

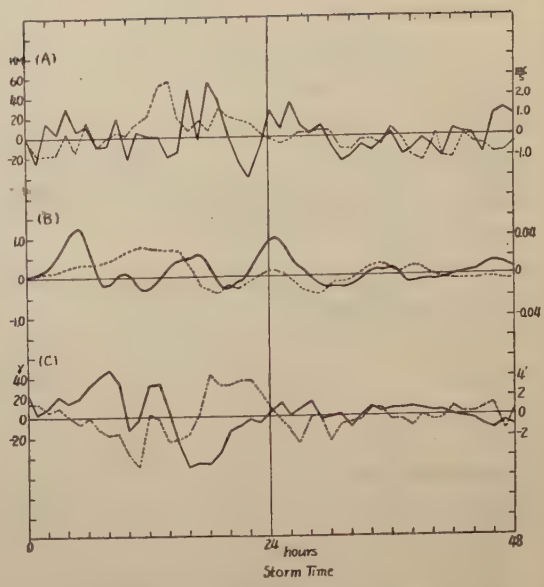

(b) Watheroo, 2^h, May 24, 1940

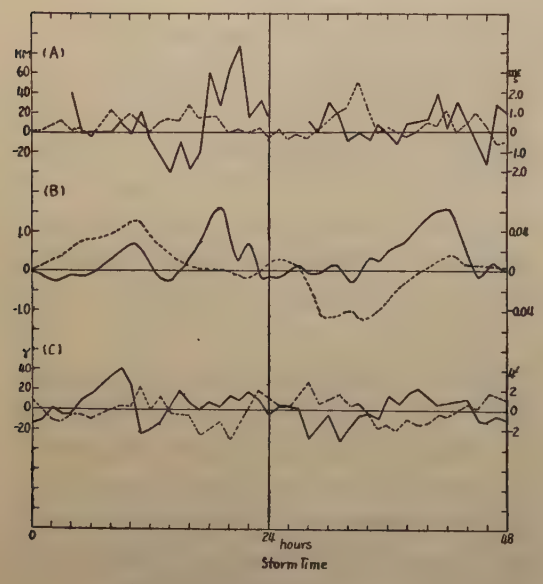

(c) Kokubunji, 9^h, Jul. 20, 1952

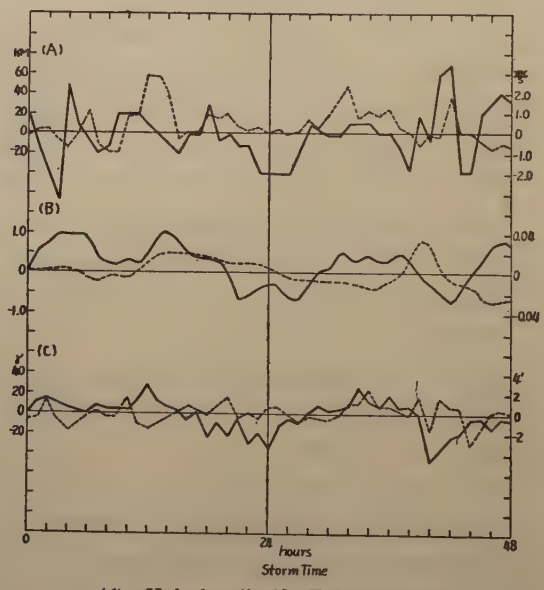

(d) Kokubunji, 1^h, Feb. 22, 1951

Fig. 7, (a)–(d) Observed and calculated deviations of individual positive disturbance. (A) represents the observed variation of Δf_0F2 (dotted line, right ordinate) and $\Delta h'F2$ (or $\Delta hpF2$ for kokubunji, full line, left ordinate) for the $F2$ disturbance which begins at the time shown below. The time is the nearest local time before the beginning of the geomagnetic storm and this time is taken as zero of the storm time. (B) represents the calculated variations of the deviations of the maximum electron density (dotted line, right ordinate) and the height (full line) and (C) the observed geomagnetic disturbance-daily variations of ΔH (full line, left ordinate) and ΔD (dotted line, right ordinate).

S_q variation (and also v_q) in that season behaves predominantly semi-diurnally [27].

6. *F*2 Disturbances in Equatorial Zone

For the comparison with the results in the sections **4** and **5** and for the later discussions, we show the observed and calculated results of the *F*2 disturbances in the equatorial zone. These results are published in another paper [9], hence the brief description is given. The study is made for the data at Huancayo during the years 1938 –1939. The electrical conductivity is taken as

$$K=1.73\times10^{-7}\ p(t)\ e.m.u \tag{9}$$

both for the quiet and disturbed days. $p(t)$ in (9) has no seasonal variation and is shown in Table 3.

Table 3 $p(t)$ *in the equatorial zone*

local time	0^h	2	4	6	8	10	12	14	16	18	20	22
$p(t)$	0.27	0.21	0.21	0.58	1.36	2.20	2.57	2.20	1.36	0.58	0.21	0·21

Some examples of the calculated and observed deviations for individual state are shown in Fig. 8 (a)–(c). In this figure parts A and B correspond to those in Fig. 6 and 7, and C represents the disturbance-daily variation of ΔH ($\simeq\Delta X$).

Most of *F*2 disturbances in the equatorial zone are the positive disturbances and it is clear that these disturbances are well accounted for in term of the vertical electron drift both for the electron density and the height and that above results are due to a fact that the velocities of the drift on the quiet and disturbed days are set up with a phase difference by about 180°.

7. Variation of *F*2 Disturbances with Season and Latitudes

In the section **2** the observed variations of the *F*2 disturbances with season and

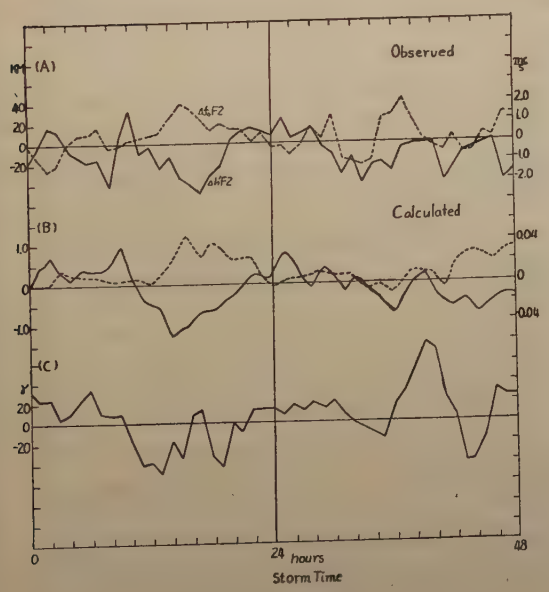

(a) Huancayo, 20^h, Jul. 2, 1939

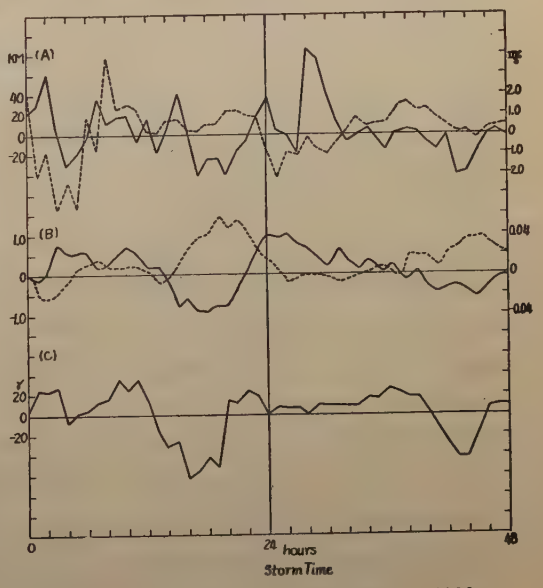

(b) Huancayo, 19^h, Jan. 4, 1939

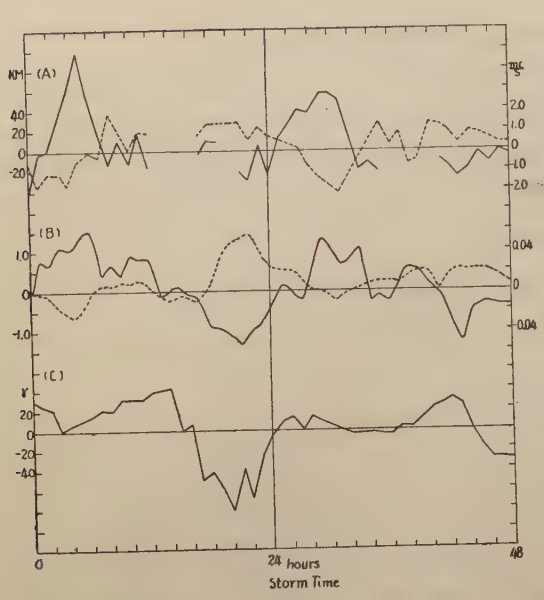

(c) Huancayo, 16^h, Feb. 13, 1938

Fig. 8, (a)-(c) Observed and calculated deviations for the $F2$ disturbance in the equatorial zone. (A) represents the observed variatons of Δf_0F2 (dotted line, right ordinate) and $\Delta h'$ $F2$ (full line, left ordinate) for the disturbance which begins at the time shown below. The time is the nearest local time before the beginning of the geomagnetic storm and this time is taken as zero of the storm time. (B) repressents the calculated variations of deviations of maximum electron density (dotted line, right ordinate) and the height (full line) and (C) the observed gomagnetic disturbance-daily variatin of ΔH.

latitude are revealed and in the sections **4,5** and **6** they are accounted for as an effect of the vertical electron drift for individual cases. In this section we discuss physically why the two types of disturbance occur, why the occurrence of them depends on the season and latitude and furthermore why the amplitude of the deviative value depends on the magnetic or sunspot activities.

Fig 9 shows the mean variation of the velocity v_q on the quiet day (dotted line) and the mean variation of the velocity v_d on the disturbed day (full line) in local summer (left hand side) and winter, at Washington, Watheroo, Kokubunji, and yearly mean vaviation of those velocities at Huancayo. From this figure it is easy to find that the velocity v_d in each station has the same phase (with the maximum downward velocity near noon). The velocity v_d in higher latitudes than Washington will have the same phase, inferring from the analysis of S_D by Vestine *et al* [22]. On

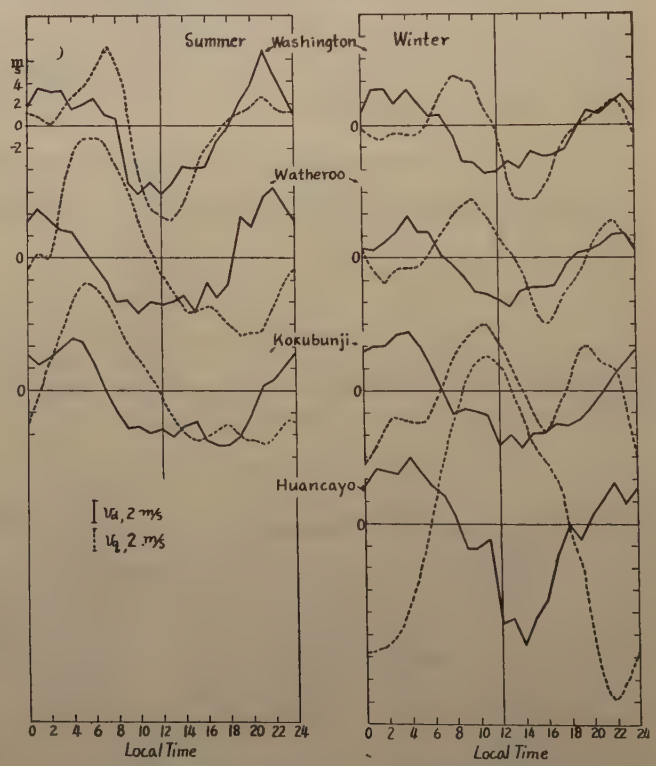

Fig. 9 Mean daily variations of the vertical drift velocities v_q (dotted line) and v_d (full line) for $F2$ disturbances used in the calculations. The variations in summer are shown in the left-hand side and those in winter and yearly mean at Huaneayo in the right-hand side.

the other hand, the velocities v_q in the four stations differ depending on the season and latitude. That is to say, in summer the velocity has the phase whose maximum downward value comes near noon at Washington, changes the phase with latitude and has a phase whose maximum upward value comes near noon at Huancayo, while in winter in middle latitude v_q varies from 0^h to 14^h analogously to that at Huancayo.

Now the maximum electron density in the moving region is lesser than that in the static region (no movement). This is well known as the geomagnetic distortion in the magnetic equator or in middle latitudes [23] [24] [25], Therefore if the velocity v_d is set up in such a way that v_d+v_q tends to zero, that is to say, that the v_d differs from v_q by 180° when their amplitudes are about the same, the moving region tends to approach to the static region and the maximum electron density increses. This representative example is the positive disturbance at Huancayo. Analogous circumstances take place partially in winter in middle latitudes as shown in Fig. 9, so that the positive disturbance also takes place in those latitudes in winter.

On the contrary, if the daily variation of v_d has the same phase as that of v_q the reduction of the maximum electron density is promoted. In this case the negative disturbance takes place. The representative example is that at Washington in summer or in equinox. For the negative disturbances in Watheroo and Kokubunji in summer, above principle may be applied, though the coincidence of the phases of both velocities is not sufficient. Since the verocity v_q is deduced from the geomagneitc S_q variation, which originate from the dynamo current in the ionophere, the latitudinal and seasonal variations of the S_q daily variation leads to the variation of v_q and to the daily variation of the $F2$ region. According to the discussions above mentioned, in the higher latitudes than the center of the S_q current system the negtive disturbance may occur, since the daily variation of the deduced v_q may coincide with that of v_d, and in lower latitudes than the center the positive disturbance is easy to occur. In summer the center of the S_q current system situates in fairly low latitudes, about in 30°, therefore in higher station than 30° the negative disturbance may occur, while in winter the center seems to situate near 40°, therefore below this latitude the positive disutrbance may predominantly occur. (though actually we must take into consideration the magnitudes of the velocities v_q and v_d as described below).

Consequently, the dependency on the latitude and season of the occurrence of the negative or the positive disturbances is ascribed to the variations of the drift velocity v_q on the quiet day with latitude and season, in other words, to the effect of the S_q dynamo current in the ionosphere.

The dependency on the geomagnatic or sunspot activities of the amplitude of the deviation and of two kinds of disturbances is explained in the following way. With the increasing geomagnetic activity the disturbance-daily variation, from which the velocity v_d is derived, increases. In this case the magnitude of v_q becomes to be negligible compared with that of v_d, so that the resultant velocity of v_d and v_q romoves

the seasonal variation and sometimes the latitudinal variation. After all, the drift velocity in the $F2$ region in the strom time becomes apparently v_d alone and the decrease of the maximum electron density results in every latitudes and seasons. The larger the geomagnetic activity, the larger is this tendency. Thus the negative disturbance is easy to occur in large geomagnetie activity.

There seems to be two reasons for the fact that in larger sunspot activity the larger (negative) deviation of the f_0F2 is caused. One of them is that in larger sunspot activity the f_0F2 itself becomes larger, therefore the decrease of the f_0F2 must be large compared with that in low value of the f_0F2, even if the decrease of the electron density has the same percentage. The other is that in larger sunspot activity the larger geomagnetic variation is easy to accur, so that the velocity v_d becomes large compared with v_q and thus the negative bisturbance tends to occur as mentioned above.

8. $F2$ Disturbances in High Latitudes

The theoretical considerations of the $F2$ disturbances at the stations in higher latitudes than Washington are not given, because of lack of the hourly values of the ionospheric or/and geomgnetic data in those stations. However, Meek [12] studied the ionospheric disturbances statistically in the high latitudes includuig the auroral zone (Canada and Alaska) for their individual states. He pointed out that the most remarkable feature of the $F2$ disturbances in these latitude is the depression of the f_0F2, whose maximum comes at noon (somtimes the second maximum depression at about 18^h). Thus the $F2$ disturbances in high latitudes are predominantly the negative disturbances. This is also known from Fig. 1 and 4 in the section **1**. Meek also pointed out that the negative variation continues for several days and that the greatest depression of the f_0F2 takes place in the southern part of the auroral zone, 60° to 65° geomagnetic latitudes, and not in the auroral zone itself. Since he did not discuss there the relation between the individual $F2$ disturbance and the corresponding geomagnetic variation, we cannot know the individual geomagnetic variation. But the general characteristics of the S_D variation in high latitudes (below the auroral zone) are similar to those in middle latitudes, as shown by Vestine *et al.* Hence the main feature of the $F2$ disturbance in high latitudes are considered to be accounted for as an effect of the vertical electron drift.

9. Discussions

(i) The effect of the electron production plays an important role on the determination of the maximum electron density and the height both on the disturbed and quiet days. However, since the production has a complicated distribution with height and varies with time, it is sometimes neglected or eliminated in the process of the calculation of the above values for the sake of simplicity. But this simplified method does not show the actual amounts, especially, for the height variation. In the sections

2, and 4 it is shown that the increment of the height in daytime on the disturbed day is not obtained. This is understood by knowing that the effect of the electron production is predominant. That is to say, the direction of the resultant velocity on the disturbed day is upwards in the early morning or sometimes throughout the morning, so that the electron mass of the maximum density moves upwards approximately with the drift velocity when the electron production is absent. But when the production begins, the accumulation of the electron at lower height than the height of the initial maximum density, increases abruptly even the electron drift is going on, and the density there becomes larger than the initial maximum. Then the density and the height to be measured are those for the lower part. This displacement of the obserbed height occurs in a few hours after the sunrise. This circumstance will be the same for the drift of the electron by any causes other than the electric field. Consequently, the value of the deviations of the maximum density and the height can be obtained only by solving the continuity equation numerically or analytically which includes the electron production.

(ii) It is found that the increase in height of the negative disturbance in daytime is not the actual variation and that as far as the height is concerned the daily variations of the deviation in most $F2$ disturbances have the same characteristic regardless of the latitude and season. Hence the statistical results for the height variation which have been previously obtained by some authors, should be reexamined because of the correction of the height variation is not made. It has been considered up to date that since the increase of the height in many disturbances is accompanied by the decrease of the electron density and *vice versa*, the inverse relation between them may be the basic fact in the $F2$ disturbance. However, this concept no longer holds.

(iii) In the statistical study of the $F2$ disturbance the deviation is often divided into two parts, *Ds* and *Dst*, by analogy to the analysis of the deviation of the geomagneyic field. However, the separation in the ionospheric case seems to be brought as results of the technical treatment of the data and the physical meaning is somewhat different from that of the geomagnetic case. According to our calculations, the vertical electron drift which has the diurnal variation causes the variations of the electron density and the height which contribute to the *Ds* and *Dst* variations. On the other hand, the electron drift which has a long period causes a variation which contributes to the two parts. These facts show that the variation in the ionospheric case differs from the electro-magnetic induction as seen in the geomagnetic field. The reason why the variation in the ionosphere is complicated is due to the fact that the variation depends on some factors in the continuity equation. From the above considerations it is premature to consider that the *Ds* and *Dst* parts of the ionospheric variation are due to the causes which have respectively the characteristics like *Ds* and *Dst*.

(iv) Besides the phase difference of the drift velocities, the mechanism of the increment of the electron density are studied. They are:—

(a) The height gradient of the drift velocity

(b) The temperature effect

(c) The electron production by impinging particles

Of these considerations, (c) may be neglected for the disturbances in middle latitudes. In winter the height of the $F2$ region on the quiet day lies in the lower level than in other seasons, so that the effect (b) may take pace, because the temperature below 300 km altitude has the gradient with the height [26]. This effect is calculated numerically with an assumption that the temperature is 600 K at 200 km and the linear increasing rate of the temperature is $5°K$/km. It is found that the effect of the temperature gradient is negligible. For the effect (a) the calculations are made for the case of the increasing velocity upwards. According to Briggs and Spencer [27], the horizontal velocity of the wind in the $F2$ region has a height gradient, of about 1m/s /km. As the wind in the $F2$ region is considered to be the motion of the charged particles due to the electric and geomagnetic fields, the motion in the vertical direction may has also a height gradient. So that the velocity seems to increase with the increasing height. The effects are calculated for the following three cases.

$$(1)\quad v=v_0\frac{z+2}{2}$$

$$(2)\quad v=v_0\ \frac{z}{2}$$

$$(3)\quad v=v_0\ (z+1)$$

where v_0 is the velocity at the reference level ($z=0$ for (1), $z=2$ for (2), and $z=0$ for (3)) and in each case the velocity below the datum level is taken to be equal to the velocity at the level. The results of the calculations do not show the remarkable increase of the electron density, except for a few hours centered on noon. When the exponential increase of the velocity with height is taken, the results seems to be worse. If the velocity decreases with the increasing height as shown by Hirono [28], the effect is not to incrcase the electron density, but to decrease.

10. Conclusions

It is recognized that the $F2$ disturbances in middle latitudes are classified in two types of disturbances, negative and positive, the former of which is the representative disturbance in high latitudes and the latter analogous disturbance to that in low latitudes or in the equator. From the numerical calculations of the effect of the vertical drift of the electron for the indivudual state, it is found that these two types of dis-

turbance can be explained by the drift theory. From the above results and the successful explanation of the $F2$ disturbance in the equatorial zone, it can be said that the negative disturbances is caused most remarkably when the phase of the daily variations of the velocities v_a and v_q are about the same and the positive disturbance caused when they are different by about 180°, and that the seasonal and latitudinal variations of the $F2$ disturbance are attributed to the seasonal and latitudinal variations of the v_q, in other words, to the S_q dynamo current from which v_q is deduced.

Acknowledgements

The author wishes to express his hearty thanks to Prof. M. Hasegawa, Dr. M. Ota and Dr. M. Hirono of the Geophysical Institute, to prof. K. Maeda of the Electronic Engineering Institute, Kyoto University, and Prof. T. Nagata and Dr. N. Fukushima of the Geophysical Institute, Tokyo University for their kind advice and valuable discussions in the course of this study. He also wishes to express thanks to the Director and the Members of the Kakioka Magnetic Observatory and to the Director and the Members of the Radio Reserch Laboratory for sending him respectively the geomagnetic and ionospheric data.

References

[1] J. H. Meek, J. Geophys. Res., **58,** 445 (1953)
[2] T. Nagata, Rep. Iono. Res. Japan, **8,** 39 (1954)
[3] D. F. Martyn, Nature, London, **171,** 14 (1953); Proc. Roy. Soc. Lon., A, **218,** 1 (1953)
[4] K. Maeda, Rep. Iono. Res. Japan, **7,** 81 (1953)
[5] M. J. Seaton, J. Atmosph. Terr. Phys., **8,** 123 (1956)
[6] L. V. Berkner, and S. L. Seaton, Terr. Mag., **45,** 393 (1940)
[7] T. Sato, J. Geomag. Geoele., **9,** 57 (1957), in this issue.
[8] T. Sato, Rep. Iono. Res. Japan., **10,** 35 (1956)
[9] T. Sato, J. Geomag. Geoele., **8,** 129 (1956)
[10] H. Ueda and Y. Arima, Rep. Iono. Res. Japan. **6,** 1 (1952); **6,** 169 (1952)
[11] E. V. Appleton, and W. R. Piggot, J. Atmosph. Terr. Phys., **2,** 236 (1952)
[12] J. H. Meek, J. Geophys. Res., **57,** 177 (1952)
[13] N. Fukushima, and T. Hayashi, Rep. Iono. Res. Japan, **6,** 133 (1952)
[14] K. Sinno, Rep. Iono. Res. Japan, **7,** 7 (1953); J. Geomag. Geoele., **6,** 120 (1954)
[15] T. Obayashi, Rep. Iono. Res. Japan, **6,** 79 (1952); **8,** 19 (1954); 8, 165 (1954)
[16] H. Kamiyama, Rep. Iono. Res. Japan, **6,** 47 (1952)
[17] T. Sato, J. Geomag. Geoele., **3,** 90 (1951)
[18] D. H. Shinn and H. A. Whale, J. Atmosph. Terr. Phys., **2,** 85 (1952)
[19] J. E. Jackson, J. Geophys. Res., **61,** 107 (1956)
[20] K. Maeda, Rep. Iono. Res. Japan, **9,** 71 (1955)

[21] G. Millington, Proc. Phys. Soc., **44,** 580 (1932)
[22] E. H. Vestine, L. Laporte, I. Lange and W. E. Scott, The Geomagnetic Field, Its Description and Analysis. Carnegie Institution of Washington, Publication 580 (1947)
[23] E. V. Appleton, Nature, London, **157,** 691 (1946)
[24] M. Hirono, and H. Maeda, J. Geomag. Geoele., **6,** 127 (1954)
[25] T. Sato, J. Geomag. Geoele., **6,** 99 (1954)
[26] H. K. Kallmann, W. B. White and H. E. Newell, J. Geophys. Res., **61,** 513 (1956) and references therein.
[27] B. H. Briggs and M. Spencer, Rep. Progr, Phys., **17,** 245 (1954) (London Physical Society)
[28] M. Hirono, Rep. Iono. Res. Japan, **9,** 95 (1955)
[29] W. G. Baker and D. F. Martyn, Phil. Trans., **246,** 283 (1953)
[30] M. Hirono, J. Geomag. Geoele., **5,** 22 (1953)

Palaeomagnetic Studies on a Quaternary Volcanic Region in Japan*

By

T. NAGATA, S. AKIMOTO, S. UYEDA, Y. SHIMIZU, M. OZIMA, K. KOBAYASHI

Geophysical Institute, Tokyo University

and

H. KUNO

Geological Institute, Tokyo University

(Read Oct. 17, 1956; Received Jun. 17, 1957)

Abstract

Palaeomagnetic studies have been conducted of the volcanic rocks in the North-Izu and Hakone volcanic region, Japan, where complete succession of lavas has been determined by one of us (H. K.). By sampling 4~7 oriented rock specimens at each of 57 sites, the period from the very beginning of the Pleistocene to Holocene has been covered. The maximum time interval between two consecutive samples may probably be not more than several tens of thousand years except that between two samples of middle to younger Pleistocene when the volcanic activity did not occur within the region concerned. Care was taken not to use the rock samples of which natural remanent magnetization may have suffered from any significant disturbances, geolgically, chemically, magnetically or otherwise. Selection of proper samples was performed according to the criteria for the stability of remanent magnetization proposed by us previously (Journ. Geomag. Geoelec., **6**, No. **4**, 1955). The major findings obtained through the present study are: 1) During the whole Quaternary age, the geomagnetic centred dipole has been fluctuating around an axis of which north pole wandered from 72°N, 86°E to 81°N, 32°W. 2) The direction of polarization of the centred dipole was reversed at a time in the earliest Quaternary, namely during the middle period of the formation of the Usami volcano.

1. Introduction

Recent investigations on palaeomagnetism have brought about many findings of great geophysical importance, especially with regards to the long controversial hypotheses of the polar wandering, the continental drift and the reversals of the geomagnetic field in the past geological time. Excellent summaries on these works are found in the publications of S.K. Runcorn [1], P.M.S. Blackett [2] and E. Irving [3]. Many authors, on the basis of their own measurements and others', have suggested that the earth's magnetic field had undergone repeated total reversals during the geological time. Such suggestions, though plausible, would be completely justified as

* Contribution from Division of Geomagnetism and Geoelectricity, Geophysical Institute, Tokyo University. Series II, No. 64.

physical truth only when the contemporeinity of reversely magnetized rocks from various localities of the world could be proved with sufficient certainty for each suggested reversals. Such absolute datings of rocks are, however, almost inaccessible at the present time. In general, the ages of rocks are determined by geological means more precisely for the younger strata. Therefore, since 1954 we have engaged ourselves with a palaeomagnetic research on a Quaternary volcanic rocks of North-Izu and Hakone volcanic region (Fig. 1), where the complete succession of lavas had been deter-

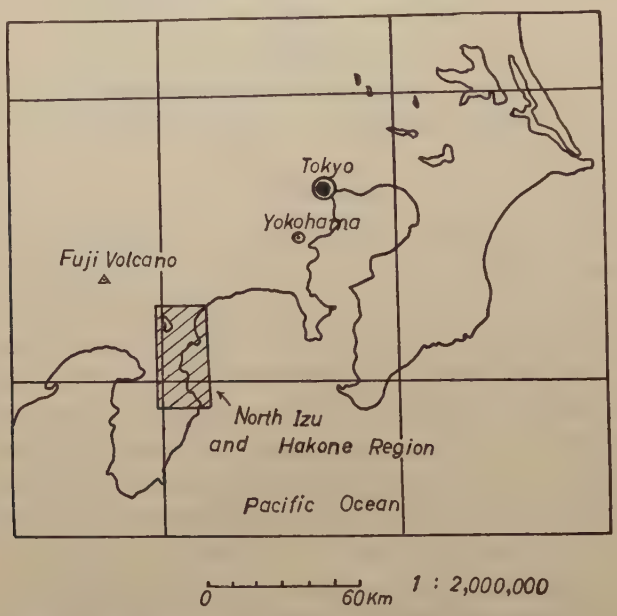

Fig. 1 Map showing the locality of the North-Izu and Hakone volcanic region.

mined by one of us (H.K.) [4], with the hope that our data would possibly be compared with the data for other parts of the world such as Iceland and France, where reversely magnetized rocks of early Quaternary were reported by J. Hospers [5], T. Einarsson and Th. Sigurgeirsson [6] and A. Roche [7]. It must here be noted that Y. Kato in 1941 conducted a palaeomagnetic research on the North-Izu and Hakone region and found that some rocks of early Quaternary and Tertiary are reversely magnetized [8].

2. Outline of the Geologic History

The region in question lies about 90 km southwest of the city of Tokyo (Fig.1). The following is a summary of the geologic history of the region already described elsewhere by H. Kuno [4]. The succession of the geologic units is shown in Table 1 and their distribution in Fig. 2.

The basement of the region is composed of older Miocene volcanic rocks named the Yugasima Group attaining to several thousand metres in thickness. Volcanic rocks ranging in age from midle Miocene to Pliocene were accumulated on this basement. In Plio-Pleistocene or older Pleistocene the central part of the present Izu peninsula

Table 1. *Stratigraphic succession of rocks of North-Izu and Hakone region and the estimated period of their eruption.*

Geologic age		10^3 years	Geologic units and their thicknesses	
QUATERNARY	Holocene	10		ŌMURO-YAMA VOLCANO GROUP
	Pleistocene	100	HAKONE VOLCANO: Central Cone lavas CC 700 m	
		200	Erosion interval	
		300	Young Somma lavas YS 300 m	
		400	Erosion interval	
		500	Old Somma lavas OS 700 m	
		600	Erosion interval	
		700	YUGAWARA VOLCANO YV 300 m	
		800	Erosion interval	
		900	TAGA VOLCANO TV 500 m	
		1000	Erosion interval	
			USAMI VOLCANO UV 300 m	
TERTIARY	Pliocene		ZYŌ FORMATION	
	Miocene		MIDDLE MIOCENE TO PLIOCENE VOLCANIC ROCKS	
			YUGASIMA GROUP	

was covered by an open sea where sediments containing mulluscan fossils were deposited (Zyō formation).

The oldest of the Quaternary volcanoes is Usami which was erupted from a centre near the present village of Usami, north of Ito. It is a stratovolcano of pyroxene andesite (designated as UV in the tables). Some of the lavas which flowed southwestward covered the Zyō formation.

Slightly later the centre of eruption moved about 10 km northward where another stratovolcano Taga was born. From this centre lavas and pyroclastic materials of pyroxene andesite were erupted in the earlier stage of activity, whereas fluidal lavas of olivine-pyroxene basalt, almost to the exclusion of pyroclastic materials, were extruded in the later stage (all designated as TV).

After a short period of erosion lava domes of dacite were erupted near the centre of Taga and also on its northwestern flank.

Then the centre of activity migrated again about 10 km north-northwestward, namely to a point near the present town of Yugawara, from which lavas and pyro-

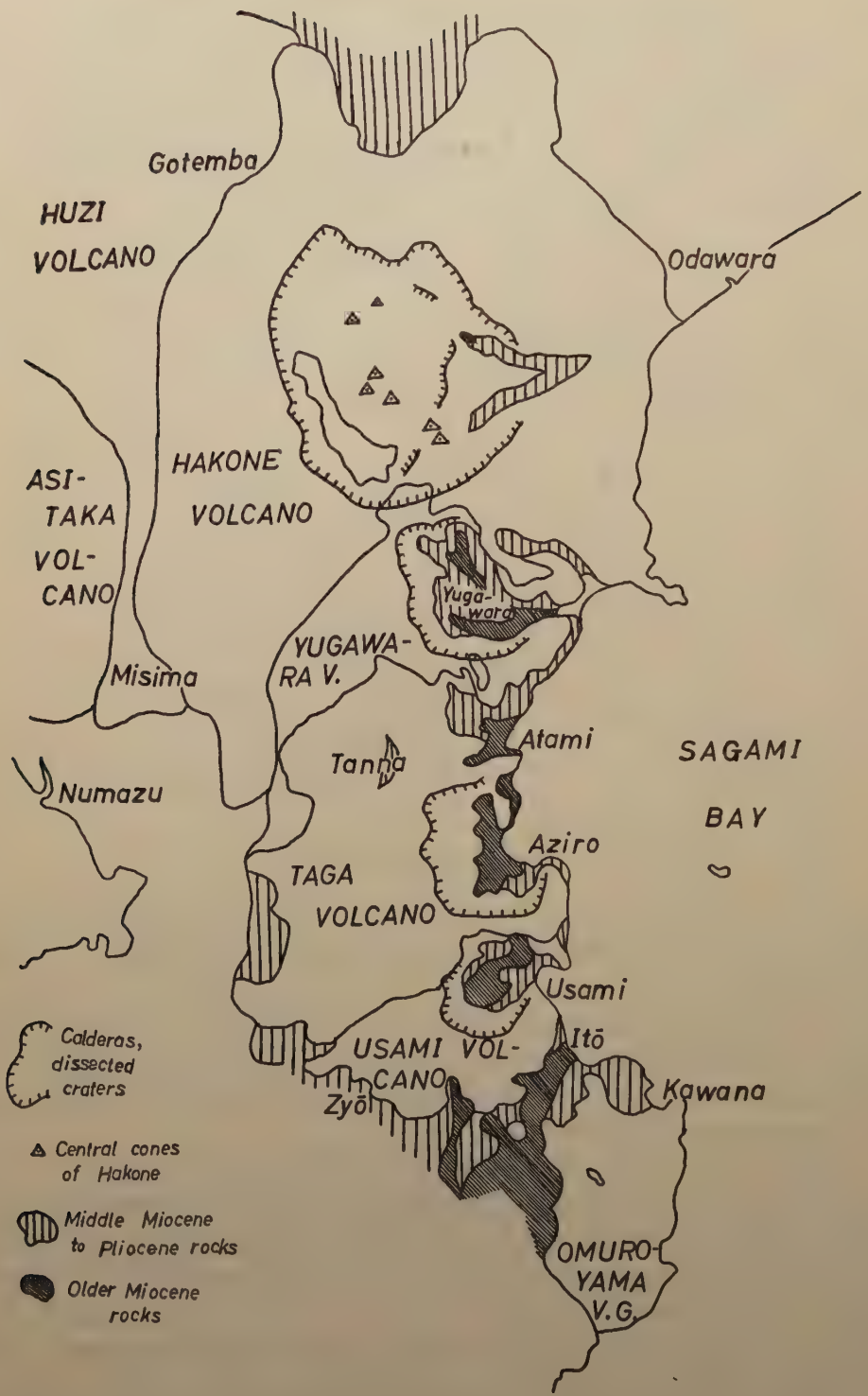

Fig. 2 Map showing the distribution of geologic units in the North-Izu and Hakone volcanic region.

clastic materials of pyroxene andesite were erupted to form Yugawara Volcano (YV).

Slightly later the activity of Hakone Volcano started from a centre situated about 10 km north-northwest of the town of Yugawara. The activity of this volcano took place in three distinct stages, the two contiguous stages having been separated from each other by periods of caldera formation and erosion.

During the first stage of activity a stratovolcano about 2700 m high was built. This eruption was caused at the outset by a magma of olivine-pyroxene basalt and later by that of pyroxene andesite. These rocks are called the Old Somma lavas (OS). Then the top of the cone subsided to form caldera measuring 11 km in NS diameter and 7 km in EW diameter. This was followed by a long period of erosion during which more than 800 m of the Old Somma lavas and the underlying Tertiary rocks in the eastern caldera wall were removed.

The second stage of activity was caused by magmas of salic pyroxene andesite and pyroxene dacite (the Young Somma lavas, YS), resulting in a gentle-sloped shield volcano within the caldera already formed. At the close of this activity a tremendous amount of pyroxene dacite magma was drained from the reservoir and produced pumice

Fig. 3 Localities of outcrops for sampling.

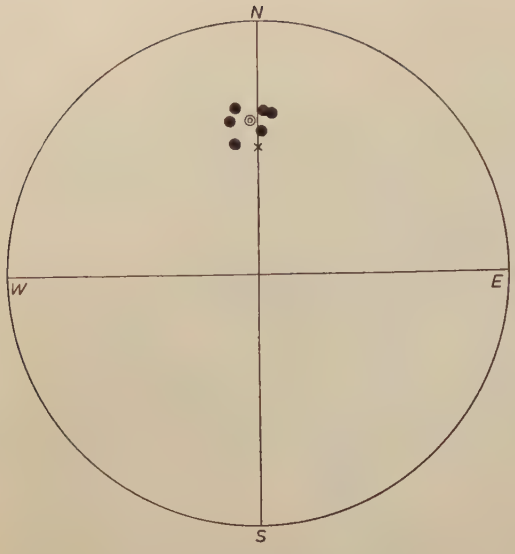

Fig. 4, a

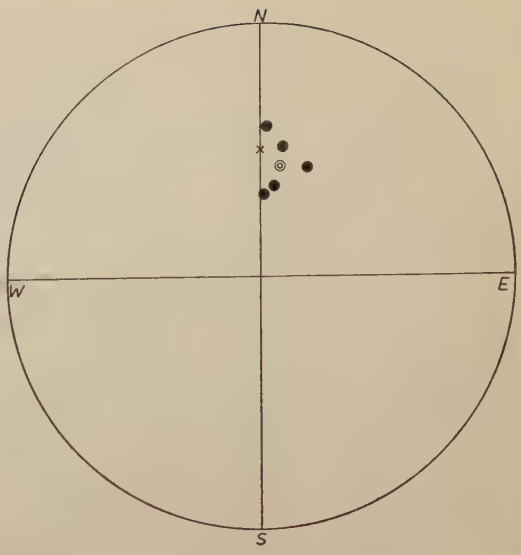

Fig. 4, b

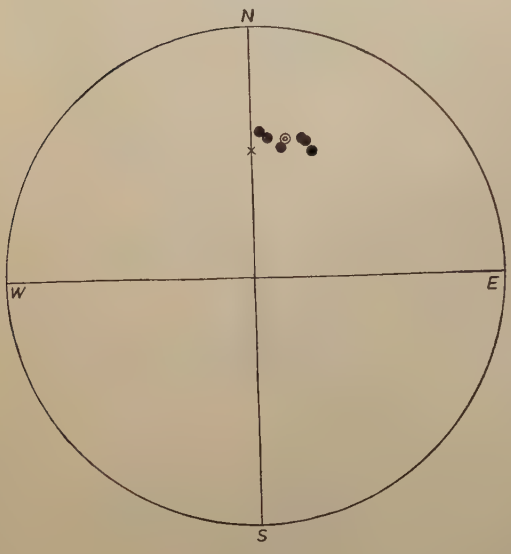

Fig. 4, c

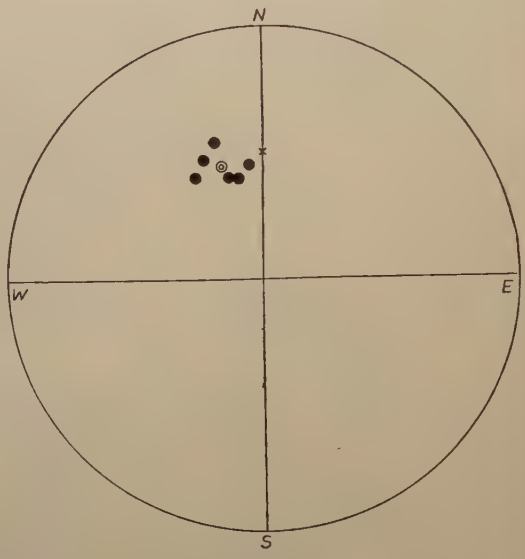

Fig. 4, d

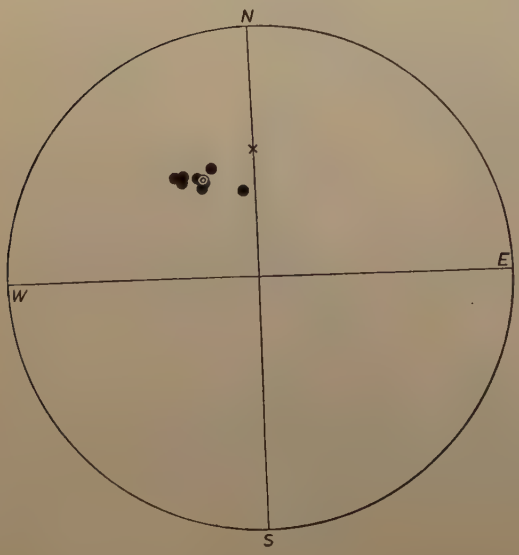

Fig. 4, e

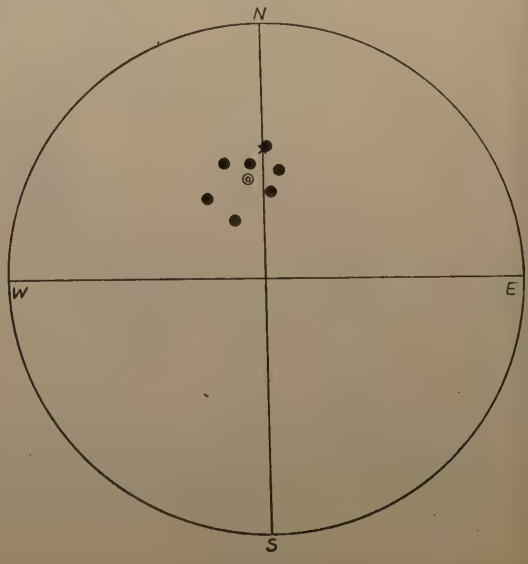

Fig. 4, f

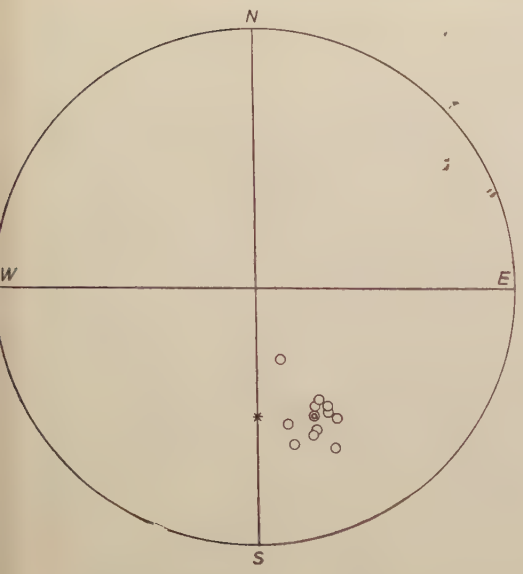

Fig. 4, g

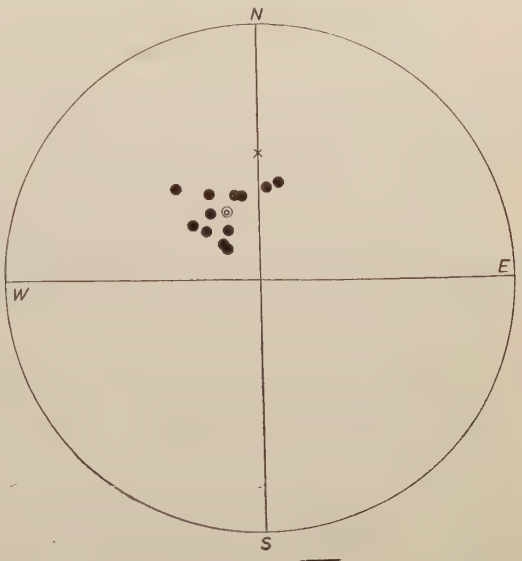

Fig. 4, h

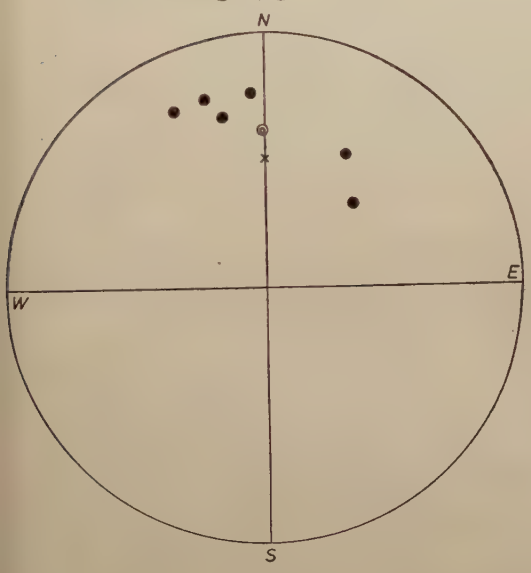

Fig. 4, i

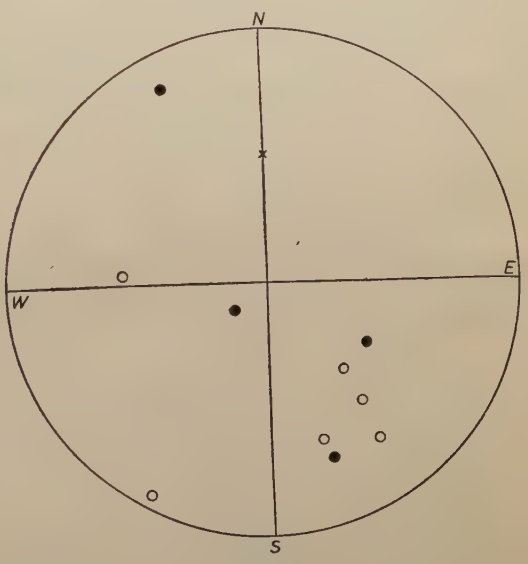

Fig. 4, j

Fig. 4, a Sample No. 26, andesite of Umenokidaira volcano.
Fig. 4, b Sample No. 9, O_{20}, andesite of Old Somma of Hakone volcano.
Fig. 4, c Sample No. 57, O_{12}, andesite of Old Somma of Hakone volcano.
Fig. 4, d Sample No. 16, D_2, pyroxene dacite at Akanezaki.
Fig. 4, e Sample No. 17, TV_5, basalt of Taga volcano.
Fig. 4, f Sample No. 15, TV_1, andesite tuff breccia of Taga volcano.
Fig. 4, g Sample Nos.18 and 45, UV, reversely magnetized andesite of Usami volcano.
Fig. 4, h Sample Nos. 20, 21 and 22, UV, normally magnetized andesite of Usami volcano,
Fig. 4, i Sample No. 3, CC_8, andesite of a central cone of Hakone volcano: example of poorer uniformity in direction of natural remanent magnetism.
Fig. 4, j Sample Nos. 44 and 46, fragmentary part of andesite of Usami volcano: direction of natural remanent magnetism is widely scattered.

Fig. 4 Examples of direction of natural remanent magnetism in Schmidt projection.
Full circle.....lower hemisphere
Hollow circle .. upper hemisphere

Double circle .. mean direction
×.....present geomagnetic north
*.....present geomegnetic south

flows. This eruption was succeeded by collapse of the centre of the shield volcano, resulting in a caldera approximating the earlier one in size and location.

After a long period of erosion which gave rise to gorges 300 m deep cutting through the eastern flank of the shield, the activity of the third stage started. Viscous magma of pyroxene andesite was extruded from vents arranged on or near an NW-SE line passing through the centre of the caldera. Six lava domes and one stratovolcano, which are called the Central Cones (CC), were formed by this activity.

The materials erupted at various stages during the growth of the Hokone Volcano are interbedded with fossiliferous sediments exposed in a region to its northeast. From stratigraphical and palaeontological data obtained from this region, it is infered that the birth of the volcano was probably middle Pleistocene. The materials of the Central Cones is interfingered with younger Pleistocene lapilli and ash from Huzi (Fuji) Volcano lying to the northwest of Hakone. It follows that the activity of Hakone lasted for the later half of the Pleistocene.

To the south of the Usami Volcano, eruption of fluidal basaltic lavas and basaltic scoriae took place during a period from younger Pleistocene to Holocene. These materials built up small lava platforms, shield volcanoes, stratovolcanoes, and pyroclastic cones within a area about 12 km in maximum diameter. These volcanoes are collectively called the Omuro-yama Volcano Group.

In Table 1 the approximate thickness of the materials composing each unit of Pleistocene is given, together with the period in 10^3 years during which each unit was formed. Each erosion period is roughly estimated in the following ways:

The lavas and pyroclastic materials of Usami, Taga, Yugawara and the Old Somma of Hakone are similar to one another in character. It is assumed therefore that each of these units was accumulated during a period proportional to the thickness of its materials. Thus the earlier half of the Pleistocene (approximately 500,000 years) is divided into three periods according to the thickness of the rocks of Usami, Taga, and Yugawara, separated by short erosion intervals. The period of the Old Somma lava eruption is also estimated according to the thickness of the rocks relative to those of the older units. As the rocks of the Young Somma and Central Cones have quite different lithologic characters from those of the older units, the periods of their eruption may not be proportional to their thicknesses. Each period is estimated as 50,000 years regardless of their thickness. The erosion period between the eruptions of the Old Somma and Young Somma lavas and that between the eruptions of the latter and the Central Cones are roughly estimated as 200,000 and 50,000 years respectively on the basis of the volumes of materials removed.

3. Results of Measurements on Natural Remanent Magnetism

Although each unit listed in Table 1 is composed of many layers of lavas and

pyroclastic materials, some of them are not suitable for the palaeomagnetic study, because they are either made up to fragments that had already been cooled through the Curie point before they came to settle at the present positions (pyroclastic rocks or fragmental parts of some lavas) or subjected to disturbances after the cooling. All samples were therefore collected from solid interior of undisturbed lava flows. One sedimentary rock is also included. These samples were selected so as to represent different horizons within each unit. On each outcrop 4 to 7 oriented samples were collected at points located more than 1 m apart from one another. The localities of these outcrops are shown in Fig. 3.

The direction and intensity of the natural remanent magnetism were measured for most samples by an astatic magnetometer, whereas those of a few samples with weak remanent magnetism were measured by a spinner type magnetometer.

Some of the results of measurements are illustrated in Fig. 4, a, b, c, d, e, f, g, h, i and j by the Schmidt projection. They illustrate the degree of concentration of measured directon of the remanent magnetism of individual specimens at a site. Fig. 4, a, b, c, d, e, f, g and h are good examples, Fig. 4, i is the example of poorer concentration and Fig 4, j shows how the directons of remanent magnetism are scattered for a group of samples collected from a fragmental part of a lava flow.

Table 2 lists the general results of measurements. The names of the geologic units and rocks refer to those in H. Kuno's paper [4].

The values of direction and intensity of natural remanent magnetism for each site and the error angles for 5% of direction were calculated from the measurements of 4 to 7 samples by Fisher's method [9]. The layers with cross marks are omitted ones on account of geologcal evidence as mentioned already. The direction of the geomagnetic centred dipole, listed in the 7th column of the Table 2, were calculated from the measured direction of the remanent magnetism. They are plotted in Fig. 5 in which the full and hollow circles stand for the north and the south poles respectively. It is noted in

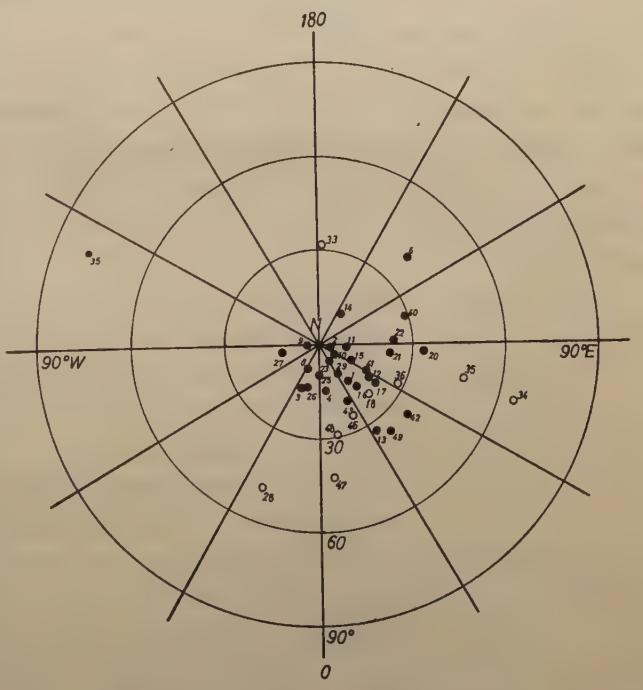

Fig. 5 Directions of geomagnetic centred dipoles deduced from the mean directions of natural remanent magnetism at each outcrops: full circle....position of north pole
hollow circle.....position of south pole
centre .....present geographic pole

Table 2 and Fig. 5 that the direction of the geomagnetic field has always been the same with that of today during the whole Quaternary age, except for a short period when some of the lavas of the Usami volcano were erupted. During this period of early Quaternary the direction of geomagnetic field was nearly reversed to that of today.

4. The Reliability Tests

As we have discussed previously [10], the palaeomagnetic study by means of the natural remanent magnetism of an igneous rock is physically justified when and only when the direction of the natural remanent magnetism is ascertained to have been kept unchanged throughout the time after the rock had been formed. From the present knowledge of rock-magnetism, the above condition may be regarded as satisfied when the natural remanent magnetism in question is proved to be the stable thermo-remanent magnetism of a stable titanomagnetite phase, produced when the rock cooled through the Curie point at the time of formation. Quite recently, the existence of stable chemical remanent magnetization and piezoremanent magnetization has been reported [11] [12]. But, their stability has not thoroughly studied yet and, besides, they are mainly concerned with the remanent magnetization of sedimentary and metamorphic rocks which we are not dealing with here. We have proposed in the previous paper that a set of practical tests should be applied on the rock specimen, when one wants to use its natural remanent magnetism for palaeomagnetic purpose. The details of the tests being described in that paper [10], we shall only briefly explain them in items here. Since the following criteria are qualitative in nature, some quantitative conditions were tentatively adopted in the present study, as shown in items 1) and 4). Symbols ○, △ and ▲ mean the "adoptable," "somewhat dubious" and "rejectable" respectively.

Notations to be used are as follows:

$J_n(T)$.....natural remanent magnetism at a temperature T.

$J_{Tc}(T)$..... thermo-remanent magnetism at a temperature T.

T_o.....room temperature.

T_c.....Curie point temperature.

J_n-T.....mode of thermal demagnetization of J_n by heating up to T and cooling down to T_o in non-magnetic space.

J_{Tc}-T ..... mode of thermal demagnetization of J_{Tc} by the same process as in J_n-T.

$(J_n)\widetilde{H}$.....mode of demagnetization of J_n by alternating magnetic field of which maximum intensity is $\widetilde{H}$.

$(J_{Tc})\widetilde{H}$..... mode of demagnetization of J_{Tc} by the same process as in $(J_n)\widetilde{H}$.

$J_s(T)$.....saturation magnetization at a temperature T.

The reliability tests

1) The ratio $J_n(T_o)/J_{Tc}(T_o)$ should be nearly equal to unity.

○.....$0.5<J_n/J_{Tc}<1.5$

△.....$0.2<J_n/J_{Tc}<0.5$ or $1.5<J_n/J_{Tc}<2.5$

▲.....otherwise

2) The modes of J_n-T and J_{Tc}-T should be similar.

3) The modes of $(J_n)\widetilde{H}$ and $(J_{Tc})\widetilde{H}$ should be similar.

4) Contained ferromagnetic mineral should exclusively be a single phased titanium-poor titanomagnetite.

○.....$T_c>400°C$

△.....$400°C>T_c>300°C$

▲.....$300°C>T_c$

5) $J_s(T)$ curve measured in vacuum should be reversible with temperature.

The results of these tests are listed in Table 2 by the symbols. As these symbols show, there is no particular indication that the naturally reversely magnetized rocks have any properties which may cause the self-reversal phenomenon. Hence, we find no reason to doubt the reversal of the geomagnetic field at the time when these rocks

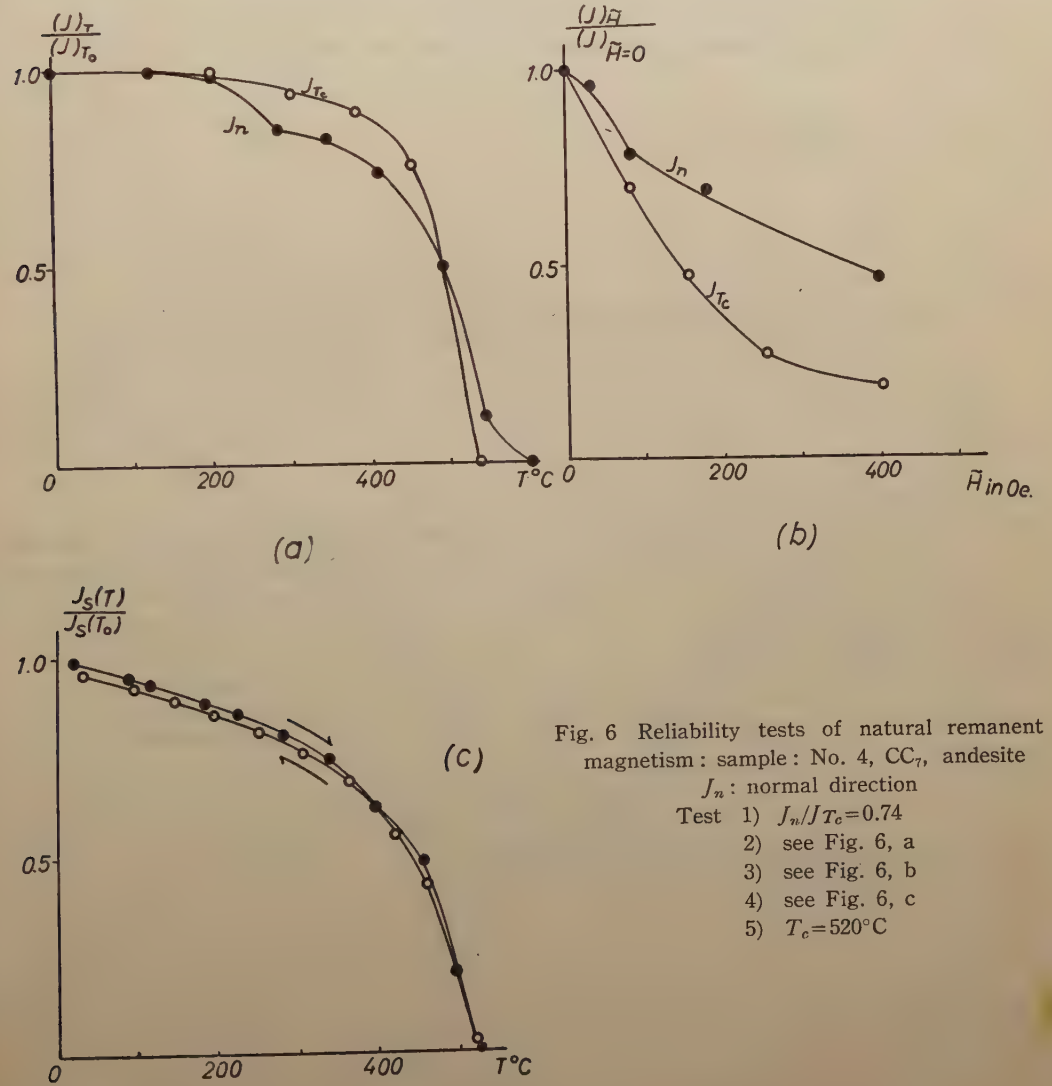

Fig. 6 Reliability tests of natural remanent magnetism : sample : No. 4, CC_7, andesite
J_n : normal direction
Test 1) $J_n/J_{Tc}=0.74$
2) see Fig. 6, a
3) see Fig. 6, b
4) see Fig. 6, c
5) $T_c=520°C$

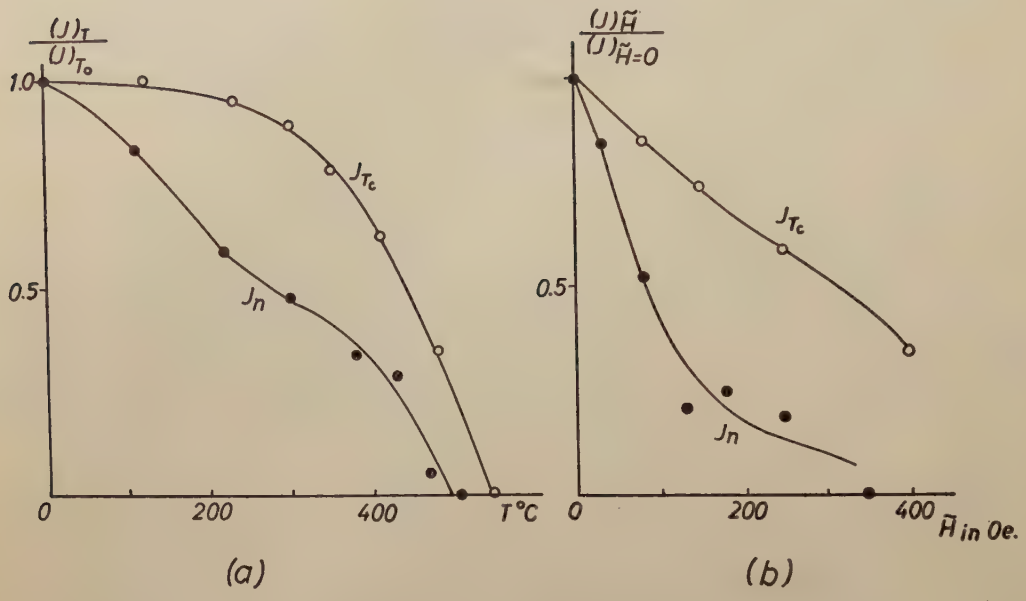

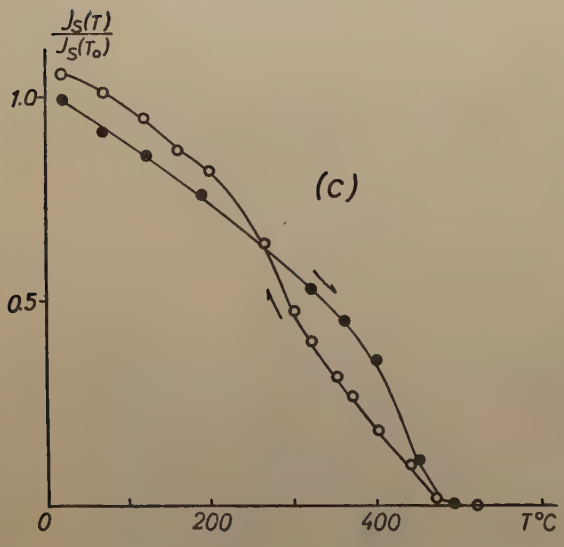

Fig. 7 Reliability tests of natural remanent magnetism : sample : No. 1, YS_3, andesite
J_n : normal direction
Test 1) $J_n/J_{Tc}=0.25$
2) see Fig. 7, a
2) see Fig. 7, b
4) see Fig. 7, c
5) $T_c=470°C$

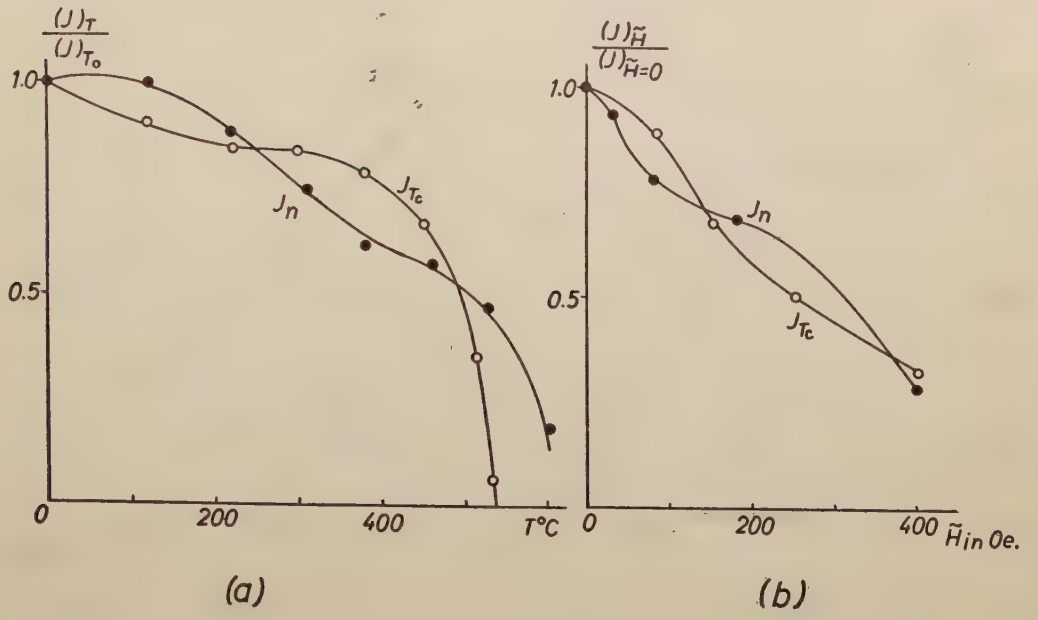

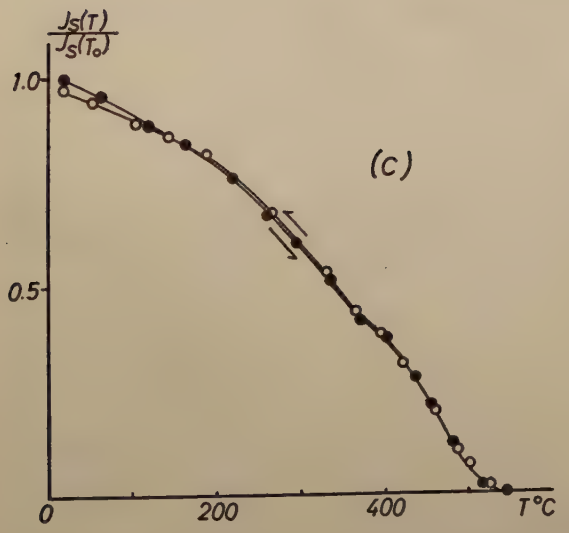

Fig. 8 Reliability tests of natural remanent magnetism : sample : No. 11, O_{18}, andesite

Test 1) $J_n/J_{T_c}=1.32$
2) see Fig. 8, a
3) see Fig. 8, b
4) see Fig. 8, c
5) $T_c=520°C$

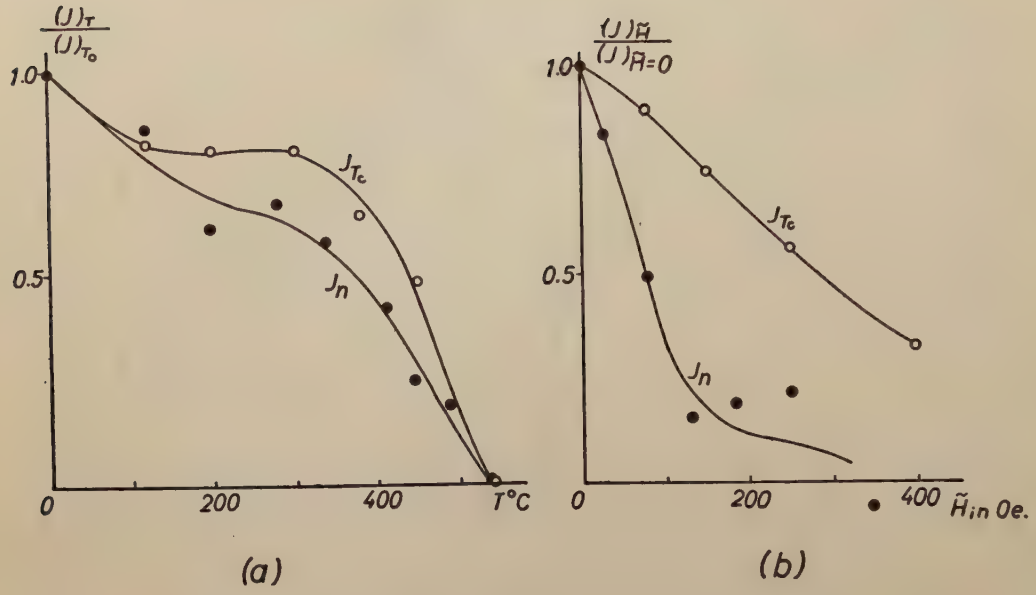

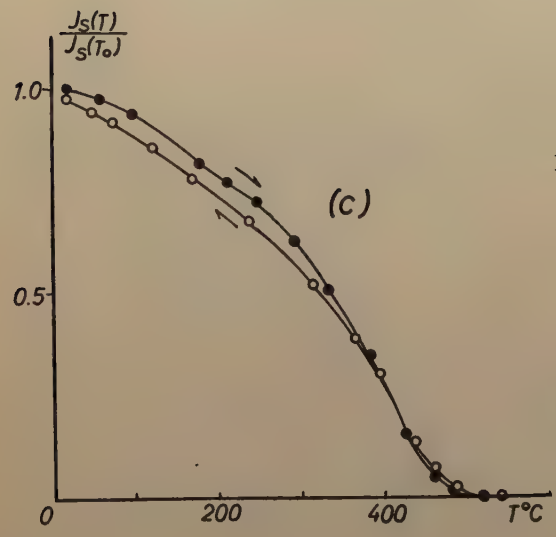

Fig. 9 Reliability tests of natural remanent magnetism : sample : No. 8, YV_1, andesite

Test 1) $J_n/J_{Tc}=0.70$
2) see Fig. 9, a
3) see Fig. 9, b
4) see Fig. 9, c
5) $T_c=480°C$

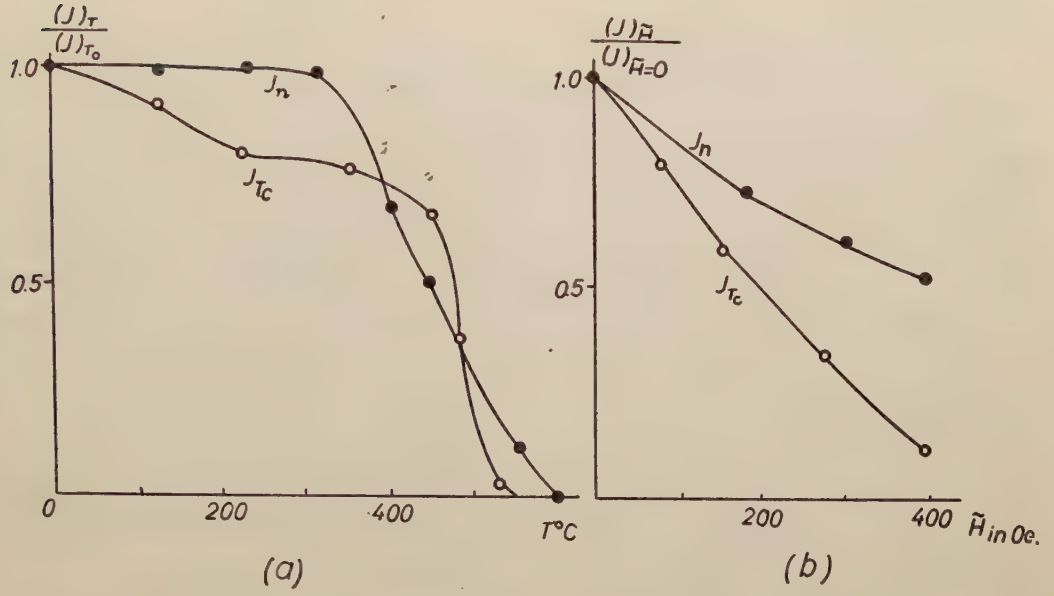

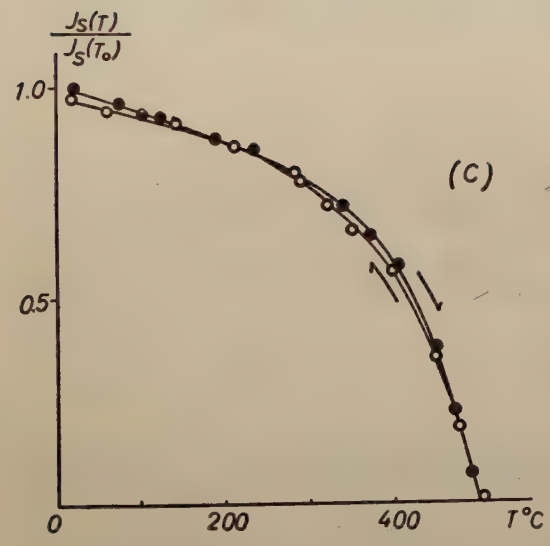

Fig. 10 Reliability test of natural remanent magnetism : sample : No. 18, UV, andesite
Test 1) $J_n/J_{T_c}=2.4$
2) see Fig. 10, a
3) see Fig. 10, b
4) see Fig. 10, c
5) $T_c=510°C$

were cooled through Curie point. Fig. 6, Fig. 7, Fig. 8, Fig. 9 and Fig. 10 are the examples of the tests performed. Fig. 10 shows the results of the tests for the reversely magnetized rock.

5. Discussion and Conclusion

The samples used in the present study cover the period throughout the Quaternary age. Any pair of samples collected from nearest horizons represents a time interval which may not exceed several tens of thousand years except those representing the horizons immediately below and above the long erosion intervals in the history of the

Hakone Volcano.

Examining the results obtained, it may reasonably be concluded from Fig. 5 that the sense of the direction of the geomagnetic field has remained the same as that of today throughout the Quaternary age, except for a short period during which a few successive lava flows of the Usami Volcano were extruded, and that the pole wandered about the neighbourhood of the present north with periods shorter than the duration of the volcanic activity which produced each unit. In order to show the more general tendency of the polar wandering during the Quaternary age, these rather rapid fluctuations are smoothed out and the value of the geomagnetic field representative of each period of volcanic activity is plotted in Fig. 11. It seems likely, judged from recent geomagnetic secular variation data and results of palaeomagnetic studies on historic and prehistoric baked earth that pseudo-periodic fluctuations of the geomagnetic pole of much shorter period and of less amplitude are superposed on this smoothed curve of general tendency. The absolute time-scale taken for abscissa of Fig. 11 is obtained as a mean value of the time range assigned to each unit given in Table 1. The value for the ordinate is the declination measured from the present geographical north and the inclination representative of each period of activity. They are obtained by averaging the values for the localities of the samples belonging to the individual periods of volcanic activity. For the Usami volcano the duration of activity was divided into three parts because of the occurrence of reversal of the geomagnetic field. Fig. 12 shows the movement of the geomagnetic north pole calculated from the values in Fig. 11; for the reversal time the south pole is plotted by a hollow circle. Viewed from the north, the pole is thus estimated to have shifted clockwise from 72°N, 86°E to 81°N, 32°W. The values shown in Fig. 11 and Fig. 12 are listed in Table 3.

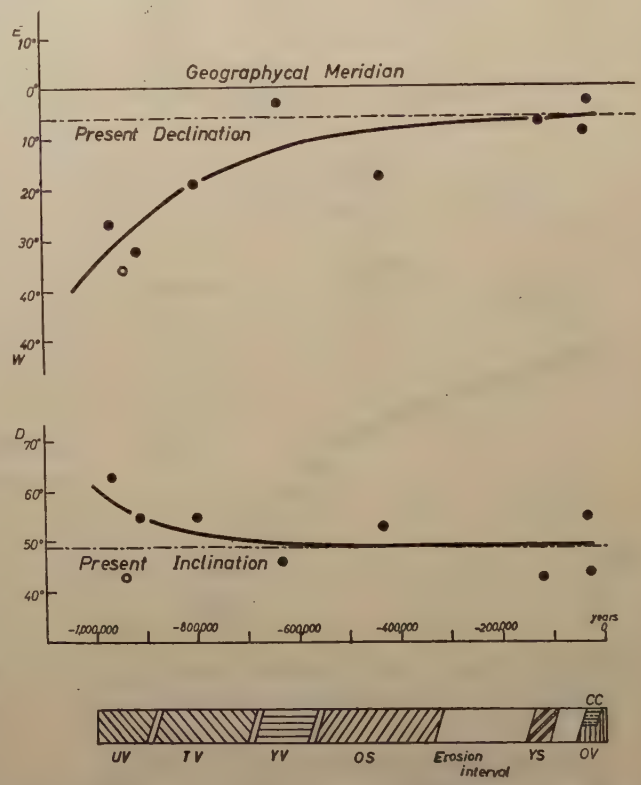

Fig. 11 Variation in the direction of geomagnetic field in the North-Izu and Hakone region through the Quaternary age, as deduced from palaeomagnetic evidence.

In order to determine the duration through which the reversal lasted, we measured the direction of natural remanent magnetization for many samples of the Usami lavas

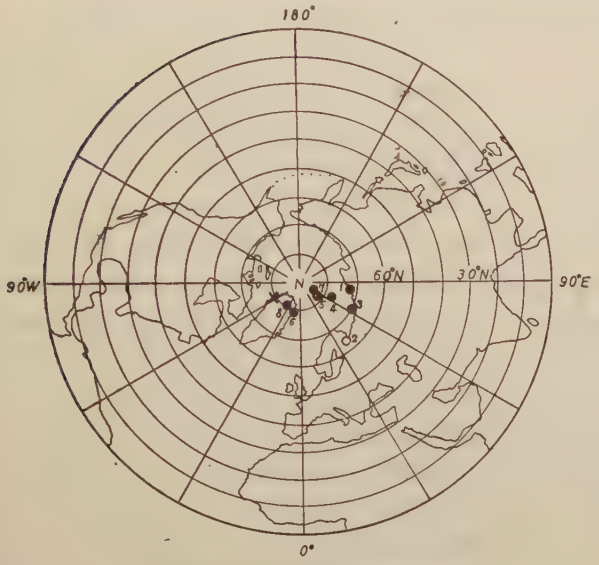

Fig. 12 Position of geomagnetic north (full circle) and south (hollow circle) pole in the Quaternary age as deduced from palaeomagnetic evidence : numbers attached to circles, as in Table 3, represent the geologic units.

(see Table 2). It is remarkable that reversal of natural remanent magnetization is found exclusively in the lava flows occurring at the middle horizon of the lava sequence of the volcano. As the duration of the activity of this volcano is estimated as about 100,000 years, the length of the duration of reversal should be a fraction of it.

It has not been possible, so far, to detect the possible change of direction of the transient geomagnetic field, in spite of our numerous measurements for the layers of lava that had considered to form the boundary between normally and reversely magnetized ones. For example, along the road-cut immediately north of Usami Tunnel,

Table 3.

No.	Volcanic activity	D_0	I_0	error angle for			Centred dipole (in geographical coordinates.)	
				p=0.05	p=0.10	p=0.50		
8	OV	−3°	44°	14°	11°	5°	81° N	32° W
7	CC	−9	55	23	19	9	86 N	65 E
6	YS	−7	43	34	11	8	79 N	13 W
	Erosion							
5	OS	−11	53	11	9	5	83 N	50 E
	YV	−3	46	–	–	–	82 N	30 W
4	TV	−19	55	20	17	8	78 N	62 E
3	UV_3	−33	55	15	13	6	70 N	61 E
2	UV_2	146	−43	29	23	13	64 S	145 W
1	UV_1	−27	63	12	10	5	72 N	86 E

northeast of the village of Usami, five successive lava flows are exposed without intervening layers of pyroclastic rocks. Complete absence of weathering products at the top of each flow strongly indicates that they were emplaced in rapid succession. All the flows but the upper-most one show the reverse direction of magnetization. The degree of uniformity of remanent magnetization of the upper-most layer is, as seen in Fig. 13, too poor to be adopted for the palaeomagnetic purpose, especially for such a critical use as a fossil of the geomagnetic field in a transient state from reverse to normal direction. The observed randomness in the direction of natural

remanent magnetization is regarded as due to the fragmentary nature of the layer.

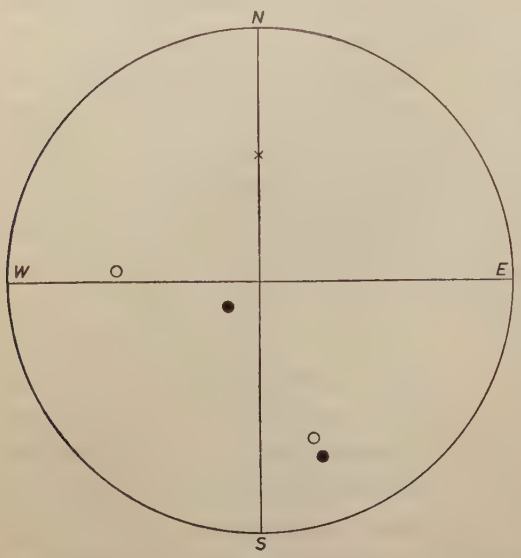

Fig. 13 Direction of natural remanent magnetism of the upper-most layer near Usami Tunnel : sample No. 44, full circle....lower hemisphere
hollow circle....upper hemisphere.

The present theoretical considerations, based on the self-exciting dynamo model of the geomagnetic field, on the other hand, suggest that the reversal of the geomagnetic field would have occurred through vanishing and development of the intensity of the dipole field without accompanied by change in direction, rather than by the migration of the axis of the dipole relative to the axis of the earth's rotation [13]. Our failure in tracing the intermediate directon of the geomagnetic field is, therefore, in agreement with these current views. We could also not find any systematic variation in the intensity of remanent magnetization of normally and reversely magnetized rocks. It may be concluded, from the result obtained so far, that the change from the normality to reversal or vice versa took place fairly suddenly in comparison with the rate of accumulation of lava flows. More detailed investigations on the remanent magnetization of rocks emplaced at the reverse-normal boundary are now in progress. Evidence of sudden reversal of remanent magnetization has recently been reported by M. Almond, J. Clegg and J. C. Jaeger for Tasmanian Tuff of Triassic age [14].

Finally, it is of much interest to compare our data with those obtained in Iceland by J. Hospers [5] and T. Einarsson and Th. Sigurgeirsson [6], and in France by A. Roche [7]. Both data seem to be in good agreement with ours in that the last occurrence of the reversal of the geomagnetic field was in the early Quaternary age. But, as for the duration of the reversal, our data obtained so far seem to suggest that it was shorter than that suggested by the data in Iceland.

References

[1] S. K. Runcorn, Adv. in Phys., suppl. Phil. Mag., **4**, No. 14, 244 (1955).
[2] P. M. S. Blackett, Lectures on Rock Magnetism, Jersalem 1956.
[3] E. Irving, Geofisica pura e appl., **33**, 23 (1956).
[4] H. Kuno, Journ. Fac. Sci., Univ. Tokyo, sec. 2, **7**, 257 (1950).
Journ. Fac. Sci., Univ. Tokyo, sec. 2, **9**, 241 (1952).
[5] J. Hospers, Koninkl. Nederel. Akad. van Wetenschappen Amsterdam, **B 56**, 467, 477 (1953).
J. Geol., **63**, 59 (1955).
[6] T. Einarsson and Th. Sigurgeirsson, Nature, **175**, 892, (1955).

Table 2.

Age	Name*	Sample Numbers	Classification of rocks	Localities	Direction D	Direction I	Error+ 5%	Direction of the centred dipole		J_n (10^{-3} emu/gr)	Reliability tests 1) J_n/J_{Tc}	2) $J_n(T)/J_{Tc}(T)$	3) $(J_n)\widetilde{H}/(J_{Tc})\widetilde{H}$	4) $J_s(T)$	5) T_c	Reliabilty§
Quaternary	Ômuro-yama volcano group															
	Ômuro volc.	27	Andesite	North-West of Ippekiko	10°	14°	14°	78° N	80° W	6.42						
	Zyôbosi volc.	25	Andesite	Near Sakasagawa	−9	47	7	80 N	0	1.27						
	Umenokidaira volc.	26	Andesite	East of Zyôyama	−9	39	6	76 N	14 W	1.32						
	Central cone of Hakone volcano															
	CC_9	×														
	CC_8	3	Andesite	Rokudôzizô	−6	38	23	75 N	22 W	3.15		○	○	○	○	○
	CC_7	4	Andesite	Motohakone	−15	44	22	75 N	7 E	1.33	0.74 ○	○	○	○	○	○
	CC_6	×														
	CC_5	2	Andesite	Asinoyu	−4	56	20	87 N	80 E	1.85	1.03 ○	○	○	○	○	○
	CC_3	×														
	CC_2	×														
	CC_1	6	Pumice	Takanosu-yama	−11	82	19	50 N	134 E	2.73	0.45 △	○	○	○	○	○
	Young somma of Hakone volcano															
	YS_5	50	Andesite	Byôbuyama	2	33	15	73 N	46 W	0.38						
	YS_3	1	Andesite	Ôhiradai	−20	51	73	75 N	38 E	0.59	0.25 △	△	△	○	○	△
	Old somma of Hakone volcano															
	O_{20}	9	Andesite	Manazuru	3	52	10	87 N	90 W	0.88	0.38 △	△	○	△	○	△
	O_{19}	11	Aphyric Andesite	Hayakawa	−12	60	18	81 N	86 E	1.35	1.32 ○	○	○	○	○	○
	O_{12}	57	Andesite	Siraisityôba	8	44	7	80 N	72 W	0.76						
	O_{11}	10	Andesite	Nebukawa	−9	55	10	84 N	60 E	0.92	0.59 ○	△	○	△	○	○
	O_5	51	Andesite	Sukumogawa	22	47	16	73 N	112 W	1.02						
	OS_1	13	Aggromerate basalt	Sengokubara	−40	38	18	57 N	33 E	5.22	0.55 ○	○	○		○	○
	OS_1	14	Aggromerate basalt	Sengokubara	3	65	16	78 N	144 E	2.03	0.80 ○	○	△		○	○
	O_2	52	Andesite	Hatazyuku	−21	47	21	75 N	28 E	0.63						
	Yugawara volcano															
	YV_2	×														
	YV_1	8	Andesite	Yugawara	−3	46	7	82 N	24 W	1.27	0.70 ○	○	△	○	○	○
	D_2	16	Pyrox. dacite	Akanezaki	−25	50	7	72 N	42 E	1.69	2.45 △	○	○		○	○
	Taga volcano															
	TV_5	17	Basalt	Aziro-Usami	−34	54	5	68 N	55 E	2.7	1.2 ○	△	○		○	○
	TV_4	49	Andesite	Kameisitôge	−46	39	12	54 N	39 E	3.78						
	TV_4	53	Andesite	Taga-oku (1)	−6	57	17	86 N	97 E	1.77						
	TV_2	54	Andesite aggromerate	Taga-oku (2)	11	49	13	82 N	98 E	0.47						
	TV_1	15	And. tuff breccia	Uomizaki	−15	57	9	79 N	65 E	0.80	0.17 ▲	○	△		○	△
	Usami volcano															
	U V	42	Andesite	Near Itô	−48	48	19	54 N	51 E	0.62						
	U V	43	Andesite	Near Itô	−24	43	28	70 N	26 E	0.70	0.63 ○	△		△	△	△
	U V	41	Andesite	Near Itô	−26	56	21	73 N	62 E	0.41						
	U V	40	Andesite	Near Itô	−32	70	6	61 N	108 E	0.49						
	U V	18	Andesite	Usami Tunnel	151	−46	12	68 S	146 W	2.58	2.4 △	○	○	○	○	○
	U V	45	Andesite	Usami Tunnel	150	−41	7	65 S	155 W	3.69	0.64 ○	○			○	○
	U V	47	Andesite	Usami Tunnel	144	−3	44	47 S	175 W	0.67						
	U V	48	Andesite	Usami Tunnel	151	−30	13	61 S	169 W	3.89						
	U V	32	Andesite	Southern cliff of Sukumo yama	114	−62	21	43 S	104 W	4.86						
	U V	33	Andesite	Southern cliff of Sukumo yama	−137	−71	31	58 S	3 W	6.29						
	U V	34	Andesite	Southern cliff of Sukumo yama	97	−53	38	25 S	107 W	1.70						
	U V	35	Andesite	Southern cliff of Sukumo yama	73	−18	15	11 N	113 W	2.92						
	U V	36	Andesite	Southern cliff of Sukumo yama	−144	−43	20	62 S	117 W	9.18						
	U V	28	Andesite	Northern cliff of Zyôyama	163	21	24	41 S	157 E	0.14	0.10 ▲	○	○	△	○	△
	U V	23	Andesite	Sakasagawa	−7	53	8	85 N	33 E	0.59		△	○		○	
	U V	20	Andesite	Siohukizaki Beach	−29	63	7	56 N	86 E	0.94	△	△	△	○	○	△
	U V	21	Andesite	Siohukizaki Beach	−32	63	19	67 N	83 E	1.12	○	○	○	○	○	○
	U V	22	Andesite	Siohukizaki Beach	−31	66	7	66 N	93 E	1.06	▲	○	○		○	△
	Zyô formations	29	Shale	Near Zyô	−15	51	16	79 N	33 E	0.46						
Tertiary	Aziro Basalt group															
	B_{4a}	12	Olivine-augite basalt	Aziro	−27	54	49	71 N	36 E	4.43	0.89 ○	○	△		○	○

* The symbols refer to those used by H. Kuno in his geologic maps attached to the paper cited.

\+ The error angles for 5% are calculated by Fisher's method.

§ Reliability for palaeomagnetic purpose.

[7] A. Roche, C. R. Acad. Sci., **233**, 1132 (1951). C. R. Acad. Sci. Paris, **243**, 812 (1956).
[8] Y. Kato, Hattori Hôkôkai Kenkyu Hôkôku, **9**, 282 (1941).
[9] R. A. Fisher, Proc. Roy. Soc., A, **27**, 295 (1953).
[10] T. Nagata, S. Akimoto, S. Uyeda, K. Momose and E. Asami, Journ. Geomag. Geoelec., **6**, 182 (1954).
[11] R. Doell, Trans. Amer. Geophys. Union, **37**, 156 (1956).
[12] N. Kawai and H. Domen, Private Communication.
[13] W. M. Elsasser, Reviews of Modern Physics, **28**, 135 (1956)
[14] M. Almond, J. A. Clegg and J. C. Jaeger, Phil. Mag., Aug. 1956, 1 (1956).

Geomagnetic Secular Variation during the Period from 1950 to 1955

By Takesi NAGATA
Geophysical Institute, Tokyo University
and Tsuneji RIKITAKE
Earthquake Research Institute, Tokyo University
(Read May 10, 1957; Received June 15, 1957)

Abstract

The geomagnetic secular variation during the period from 1950 to 1955 is estimated on the basis of annual mean values of the geomagnetic field at some seventy magnetic observatories distributed all over the earth. Judging from the spherical harmonic analysis of the variation, it seems likely that the magnetic moment of the earth's dipole is still decreasing.

1. Introduction

The question of whether or not the magnetic moment of the earth's dipole has recently begun to increase is of general geophysical interest and has been discussed by C. Gabier-Puertas [1], E. C. Bullard [2] and H. G. Macht [3]. On the basis of his extensive analysis [4], E. H. Vestine [5] showed that the rate of the decrease of the axial component of the earth's magnetic moment becomes small after its maximum around 1920. On extrapolating his result, it has been suggested that the decreasing rate might become zero at some time around 1950 resulting in an increase of the moment after that epoch.

Vestine's analysis of the geomagnetic field at epochs of every ten years has also been the source of various studies related to the geomagnetic secular variation such as the westward drift, the electric current systems on the surface of the earth's core, the shielding effect of the earth's mantle and so on. In view of such geophysical significance of the geomagnetic secular variation, it will be of some use to make clear the recent status of the geomagnetic field, because some ten years have past since the last epoch of Vestine's analysis.

One of the writers (T. N.) has been appointed as chairman of the Special Committee on Secular Variation and Palaeomagnetism, International Association of Geomagnetism and Aeronomy since 1954. At his request, some fifty magnetic observatories kindly sent him the annual mean values of the three geomagnetic components during the period from 1945 to 1955. The writers can also add some additional data published elsewhere [6], [7], [8]. The total number of observatories whose data can be used to investigate the secular variation during the period from 1950 to 1955, amounts to as many as 68, so that the writers would here like to analyse the data in the customary way. The locations of these observatories are shown in Fig. 1.

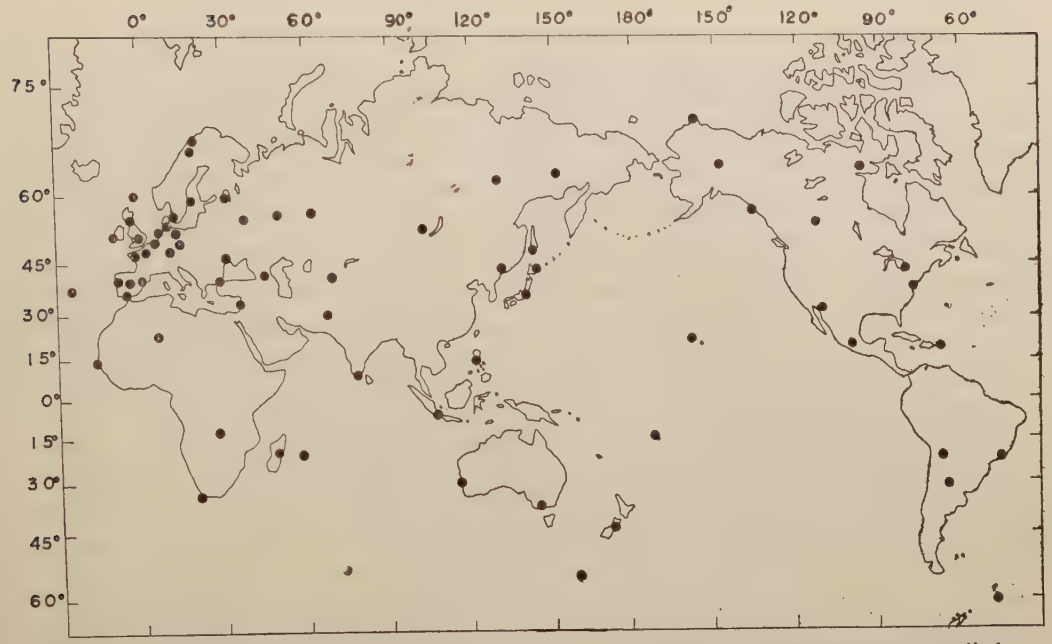

Fig. 1. The distribution of the magnetic observatories from which the data are supplied.

Table I. *The changes in the three elements of the earth's magnetic field at respective observatories.* (*Unit* : *gammas*)

Observatory	Geographic latitude	Geographic longitude	ΔX	ΔY	ΔZ
Point Barrow	71.°3	203.°2	138	− 14	65
Tromsö	69.7	18.9	22	128	148
Abisko	68.4	18.8	− 15	−127	133
College	64.9	212.2	94	− 7	—
Baker Lake	64.3	263.9	124	26	− 33
Srednikan	62.4	152.3	80	−138	− 32
Yakutsk	62.0	129.7	84	−168	178
Lerwick	60.1	358.8	108	135	116
Voeikovo	60.0	30.7	2	126	199
Lovö	59.4	17.8	33	144	132
Sitka	57.0	224.7	85	− 28	− 30
Sverdlobsk	56.7	61.1	− 9	60	290
Rude Skov	55.8	12.4	56	158	118
Kazan	55.8	48.8	− 10	77	179
Moscow	55.5	37.3	− 9	−108	193
Eskdalemuir	55.3	356.8	145	153	56
Meanook	54.6	246.7	160	− 9	—
Wingst	53.7	9.1	72	170	100
Witteveen	52.8	6.7	91	178	123
Irkutsk	52.5	104.0	55	−122	170
Niemegk	52.1	12.7	67	175	150
Valentia	51.9	349.7	227	138	171
Abinger	51.2	359.6	139	177	60

(*Table* I *continued*)

Observatory	Geographic latitude	Geographic longitude	ΔX	ΔY	ΔZ
Manhay	50.°3	5.°7	124	215	107
Průhonice	50.0	14.6	60	177	145
Fürstenfeldbruck	48.2	11.2	74	195	116
Chambon-la-Forêt	48.0	2.3	147	201	59
Nantes	47.3	358.4	174	203	72
Yuzhno Sakhalinsk	46.9	142.7	103	−119	18
Odessa	46.8	30.9	12	100	246
Memambetsu	43.9	144.2	86	−42	−84
Agincourt	43.8	280.7	131	1	−144
Vladivostok	43.1	131.9	83	−64	—
Dusheti	42.1	44.7	18	49	260
Keles	41.4	69.2	175	−19	277
Istanbul-Kandilli	41.1	29.1	46	134	254
Ebro	40.8	0.5	163	241	−2
Coimbra	40.2	351.6	235	225	−16
Toledo	39.9	355.9	240	234	−2
Cheltenham	38.7	283.2	192	−67	−101
S. Miguel	37.8	334.3	378	107	−199
San Fernando	36.5	353.8	240	259	−89
Kakioka	36.2	140.2	121	−38	−7
Ksara	33.8	35.9	96	83	315
Tucson	32.2	249.2	−20	−67	−182
Quetta	30.2	66.9	200	−29	125
Tamanrasset	22.8	5.5	180	75	−34
Honolulu	21.3	201.9	−96	−24	14
Teoloyucan	19.8	260.8	−10	−74	50
San Juan	18.4	293.9	71	−230	−504
Muntinlupa	14.4	121.0	92	−146	−148
Dakar M'Bour	14.4	343.0	249	255	−550
Kodaikanal	10.2	77.5	63	−59	−93
Kuyper	−6.0	106.7	126	−36	—
Elisabethville	−11.7	27.5	−177	70	−32
Apia	−13.8	188.2	43	184	126
Tananarive	−18.9	47.5	−254	−247	−169
Mauritius	−20.1	57.6	35	−259	−158
La Quiaca	−22.1	294.4	−285	−282	−654
Vassouras	−22.4	316.4	−359	−198	−367
Watheroo	−30.3	115.9	24	30	−154
Pilar	−31.7	296.1	−335	−251	21
Hermanus	−34.4	19.2	−306	93	452
Toolangi	−37.5	145.5	−91	152	−59
Amberley	−43.2	172.7	−88	193	101
Heard Is.	−53.0	73.4	−187	−220	−490
Macquarie Is.	−54.5	159.0	−202	152	90
Orcadas del Sur	−60.7	315.1	−333	−70	463

2. Data

From the annual mean values reported from each observatory, the changes in the north (X), east (Y) and vertical (Z) components during the period from 1950 to 1955 are calculated as shown in Table I together with the geographical latitude and longitude of the observatories. Most of the values of X and Y are deduced from the data reported as those of horizontal intensity (H) and declination (D), while very few observatories reported the values of Z as combinations of H with inclination (I). For certain observatories, extrapolations or interpolations are necessary in order to calculate the values at the epochs required though the errors due to these procedures would seldom exceed a few gammas.

3. Secular variation for the period 1950–1955

The mean secular variation for the period 1950–1955 thus calculated is shown in three charts respectively for $\dot{X}$, $\dot{Y}$ and $\dot{Z}$ as can be seen in Figs. 2a, 3a and 4a. In order to compare these charts to those of Vestine's study for 1942.5, similar charts are reproduced from Vestine's results as are also shown in Figs. 2b, 3b and 4b for respective components.

On examining these figures, we see that the general mode of the secular variation is not greatly different for both the epochs, though there can be seen some difference especially in $\dot{Z}$. In Fig. 2a, we see three vortices for $\dot{X}$ centred at the North and South Atlantic Ocean and North India. The locations of these vortices are almost the same as those of Fig. 2b though the maximum intensities at their centres have changed within a range of a few tens of gammas per year. The negative centre which has been shown by Vestine in the southern part of the Indian Ocean seems to disappear. The distribution of $\dot{Y}$ is also nearly the same as that of the Vestine's epoch as can be seen in Figs. 3a and 3b. The positive centre in North Africa and the negative ones near Madagascar and in South America still continue their activities, while the positive centre in the South Pacific seems likely to shift to the north somewhere around New Zealand. As for $\dot{Z}$ in Figs. 4a and 4b, the positive centre in the Middle East is still alive though the intensity becomes nearly one half. The negative in the Atlantic has moved to the north-west direction. We also see that the enormous positive extending from South Africa to the South Pacific around the Antarctica keeps its activity. Although the negative in the Indian Ocean seems to move to the south, no conclusive discussion is possible because of the low accuracy of the data around this region as has been pointed out by Vestine.

It is also interesting to compare Figs. 2a, 3a, and 4a to the non-dipole field for 1945 which has been graphically shown by E. C. Bullard *et al* [9] by use of Vestine's analysis. Most of the highs and lows of each component of the non-dipole field have been generally intensified during recent years. But the centres of the secular variation do not agree with these highs and lows. There is a marked tendency for the centres of the secular variation to occur at places to the west of the highs and lows of the

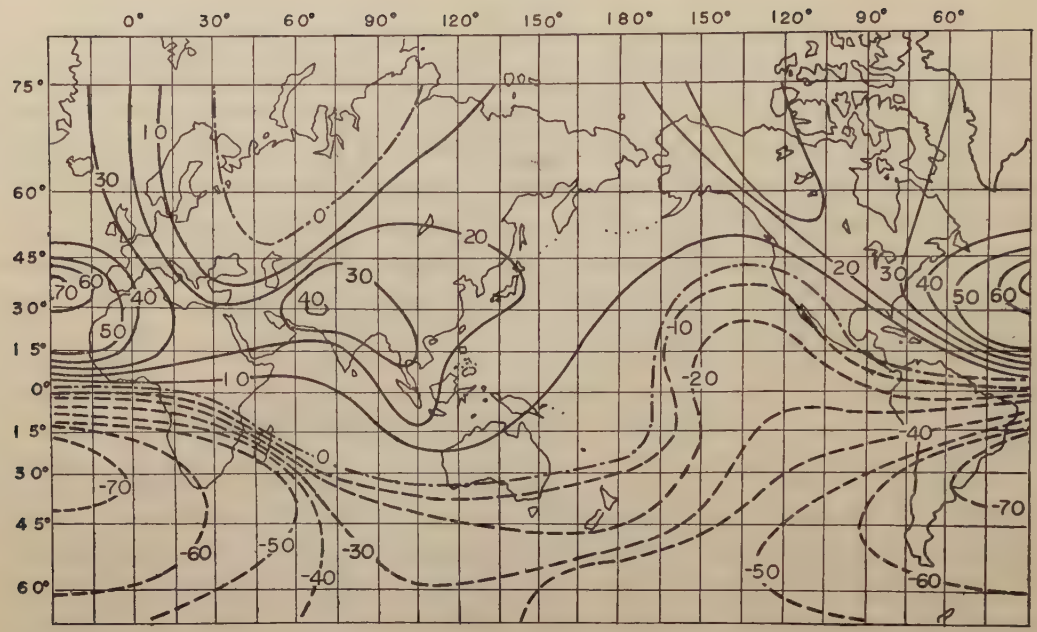

Fig. 2a. Secular vrriation for the period 1950–1955, north component, contour interval 10 gammas per year.

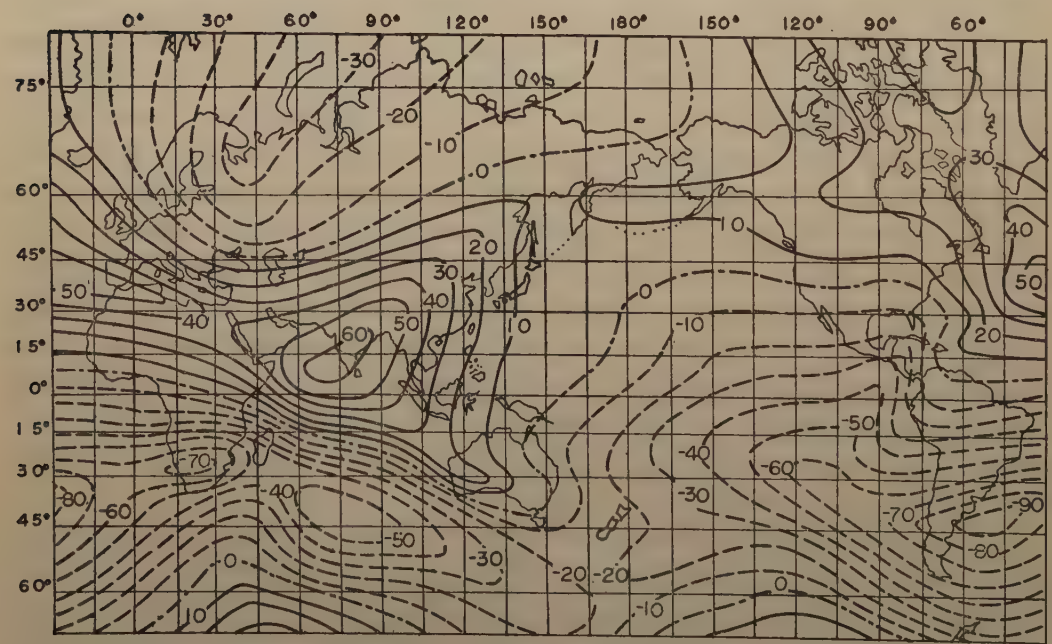

Fig. 2b. Secular variation for the period 1940–1945, north component, contour interval 10 gammas per year. (Reproduced from Vestine's result.)

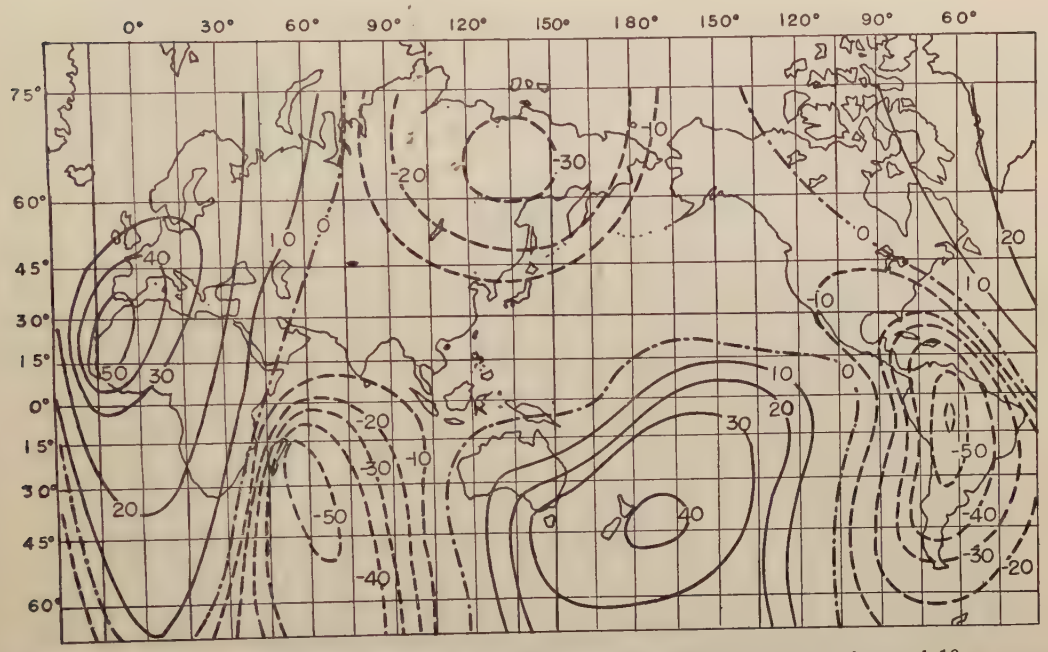

Fig. 3a. Secular variation for the period 1950–1955, east component, contour interval 10 gammas per year.

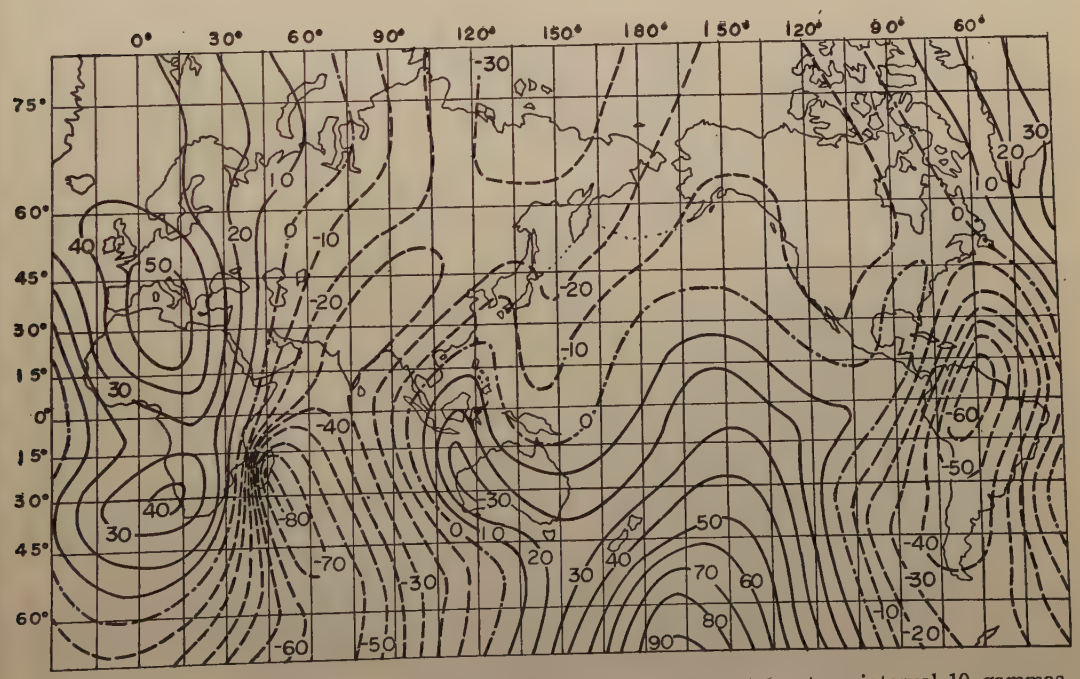

Fig. 3b. Secular variation for the period 1940–1945, east component, contour interval 10 gammas per year. (Reproduced from Vestine's result.)

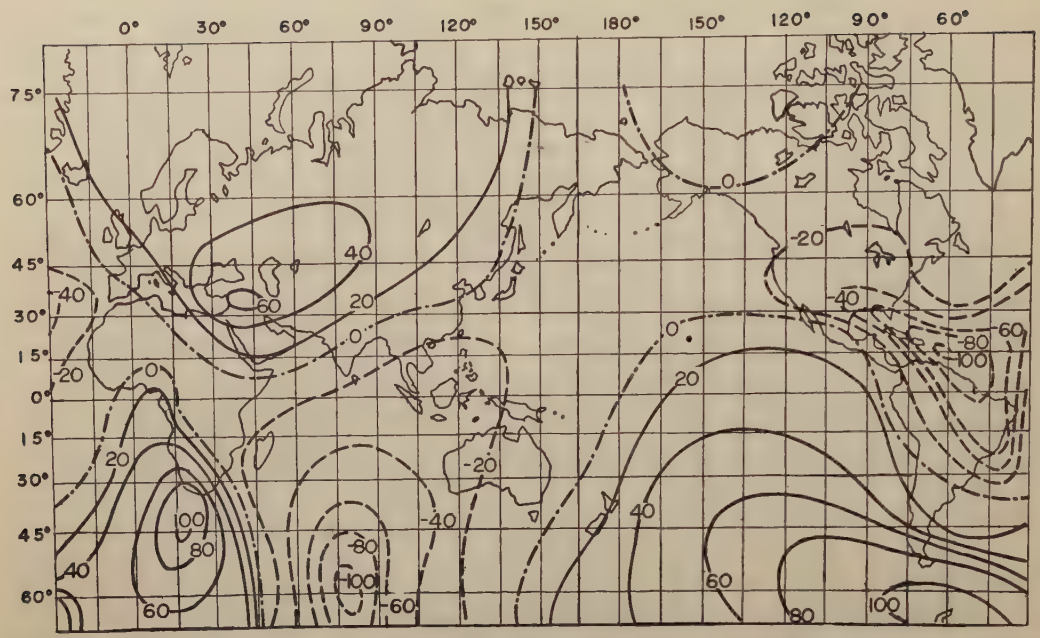

Fig. 4a. Secular variation for the period 1950–1955, vertical component, contour interval 20 gammas per year.

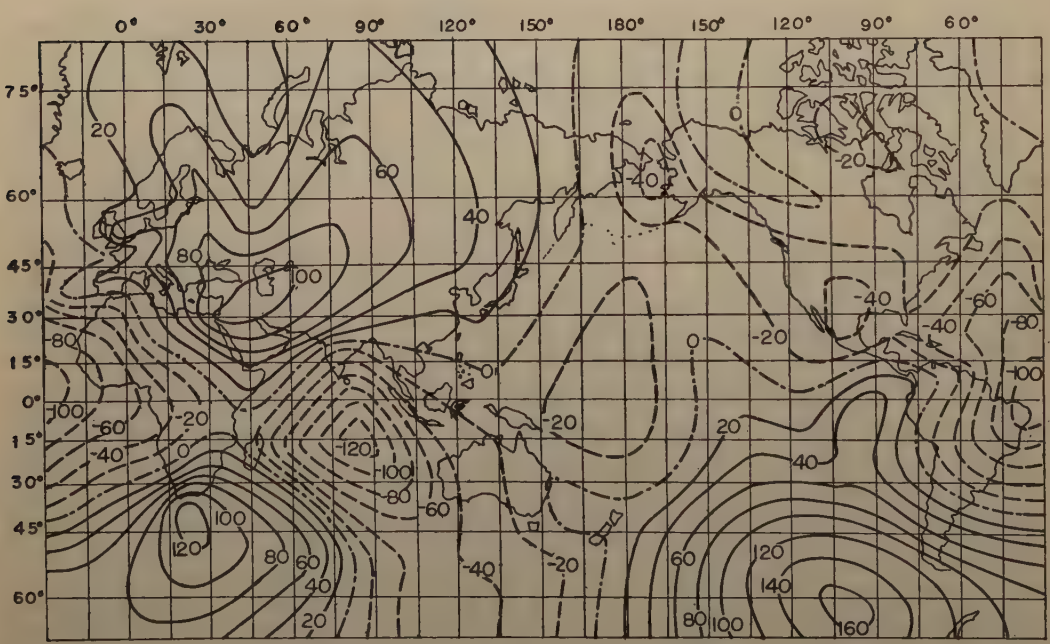

Fig. 4b. Secular variation for the period 1940–1945, vertical component, contour interval 20 gammas per year. (Reproduced from Vestine's result.)

non-dipole field. The fact can be interpreted as the westward drift of the geomagnetic field as has been pointed out by a number of geomagneticians. However, no attempt to estimate the velocity of westward drift will be made in this paper, because the velocity is so small that such a short period as that covered by the present analysis would not give any significant results.

4. Spherical harmonic analysis of the secular variation

From Figs. 2a, 3a and 4a, the amounts of the secular variations for each component are read off at the intersection points of the meridians of every 30° and the parallel circles of every 15°. Using these values, spherical harmonic analyses are conducted in the customary way. The time-derivatives of the Gaussian coefficients can be calculated independently from the combination of $\dot{X}$ and $\dot{Y}$ and $\dot{Z}$, the results being shown in Table II together with the previous analyses by many authors.

Table II. *Spherical harmonic amplitudes of the secular variation for various epochs.*

	Dyson-Schmidt	Bartels	Carlheim-Gyllensköld	Vestine-Lange				Nagata-Rikitake	
	1922–1885	1920–1902	1920–1902	1912.5	1922.5	1932.5	1942.5	1955–1950	
								X&Y	*Z*
$\dot{g}_1^0$	20	42	0	25	28	23	9	9	6
$\dot{g}_1^1$	− 1	− 9	13	1	4	1	2	0	2
$\dot{h}_1^1$	− 1	12	4	− 7	− 7	− 5	1	4	− 1
$\dot{g}_2^0$	−10	− 7	0	− 7	−10	−14	−18	−25	− 8
$\dot{g}_2^1$	6	8	− 4	− 1	1	1	0	0	− 1
$\dot{h}_2^1$	−14	−25	−12	− 9	−14	−18	−20	−17	−16
$\dot{g}_2^2$	21	13	13	24	17	10	2	4	− 3
$\dot{h}_2^2$	−18	− 8	−17	−17	−17	−14	−14	−14	−11
$\dot{g}_3^0$				6	7	4	2	6	− 2
$\dot{g}_3^1$				− 6	− 7	− 7	− 7	0	− 3
$\dot{h}_3^1$				− 6	− 5	− 5	− 1	0	3
$\dot{g}_3^2$				− 1	− 2	1	3	1	2
$\dot{h}_3^2$				3	3	4	4	7	− 1
$\dot{g}_3^3$				13	7	3	0	− 1	− 6
$\dot{h}_3^3$				−11	−11	−13	−10	− 8	− 2

(*Unit : gammas per year*)

As is seen in the table, the coefficients deduced from $\dot{Z}$ agree fairly well with those from the combination of $\dot{X}$ and $\dot{Y}$. Since the data concerned are supplied only from permanent magnetic observatories, the coefficients which are deduced from the vertical component are thought fairly reliable though they have been regarded as less accurate in the previous analyses.

5. Discussion

Now we are in a position to compare the present result to that of the previous analyses. In an extensive investigation on all the spherical harmonic analyses available by 1945, however, P. Mauersberger [10] has emphasized the fact that no one analysis is strictly comparable with another. In fact, the difference of the source of magnetic data, the method of computation and so on would result in some difficulties in comparison of different analyses. As far as the relatively large coefficients are concerned, however, two analyses by different authors, for instance, the analysis by Vestine for 1940–1945 and the present one, may be compared with one another in spite of the above difficulties.

Since the mode of distribution is not greatly different as can be seen in Figs. 2~4, the coefficients for both the analyses should agree fairly well with one another. In reality, we see in Table II that the relatively large coefficients such as $\dot{g}_1^0$, $\dot{g}_2^0$, $\dot{h}_2^1$ and $\dot{h}_2^2$ are in good agreement for both the analyses. Attention should be paid to the fact that $\dot{g}_1^0$ is the same in both the analyses, so that the decreasing rate of the axial component of the earth's dipole is to be the same for both the epoch. Even if possible errors of the coefficients are taken into account, it is of extreme doubt that the strength of the earth's dipole began to increase some time after 1950.

6. Conclusion

The analysis of the secular variation of the earth's magnetic field for 1950–1955 shows that its general tendency is nearly the same as that for 1940–1945. It is most unlikely that the strength of the earth's magnetic moment has been increasing some time after 1950. Instead, it seems still decreasing with a rate nearly equal to that for 1940–1945.

The writers are grateful to all the members of the magnetic observatories who kindly supplied magnetic data to the writers. The writers also wish to express their thanks to Miss E. Nakagawa who assisted them in numerical work as well as in preparing drawings.

References

[1] C. Gabier-Puertas, Geofisica Pura e Appl., **23,** (1952), 6.
[2] E. C. Bullard, J. Geophys. Res., **58,** (1953), 277.
[3] H. G. Macht, J. Geophys. Res., **59,** (1954), 369.
[4] E. H. Vestine, I. Lange, L. Laporte and W. E. Scott, Carnegie Inst. Pub. No. **580,** (1947).
[5] E. H. Vestine, J. Geophys. Res., **58,** (1953), 127.
[6] J. A. Fleming and W. E. Scott, Terr. Mag., **53,** (1948), 199.
[7] H. F. Johnston, J. Geophys. Res., **56,** (1951), 431.
[8] H. F. Johnston, J. Geophys. Res., **61,** (1956), 273.
[9] E. C. Bullard, C. Freedman, H. Gellman and J. Nixon, Phil. Trans. Roy. Soc. London A, **243,** (1950), 67.
[10] P.Mauersberger, Geophys. Inst. Potsdam, Abh. No. **5,** (1952), 5.

On Magnetic Susceptibility of Olivines*

By T. NAGATA, T. YUKUTAKE and S. UYEDA

Geophysical Institute, Tokyo University

(Read on May 12, 1957; Received on June 23, 1957)

Abstract

The magnetic susceptibility of several olivines, $x\mathrm{Fe_2SiO_4}\cdot(1-x)\mathrm{Mg_2SiO_4}$ with varying x has been measured. The results showed that the olivines are paramagnetic and that their molecular magnetic susceptibility χ_{mol} can be expressed empirically by $\chi_{mol}=2x\times10^{-2}$ $^{emu}/_{mol}$ at the room temperature. Using the accepted values of the Bohr magneton number of Fe^{+2} ion, and assuming that the Fe^{+2} ions are embedded isolatedly in the crystal, the paramagnetic susceptibility of olivines at the room temperature can be calculated as $\chi_{mol}=2.2\,x\sim2.6x\times10^{-2}$ $^{emu}/_{mol}$, provided that the other constituents such as Mg^{+2} and SiO_4 are only diamagnetic. The comparison of the empirical and the calculated values seems to justify the above simple calculation. We expect such calculation will also valid for other rock-forming paramagnetic minerals.

1. Introduction

It is now an established fact that the magnetic properties of rocks relevant to geophysical phenomena are principally attributable to those of the ferromagnetic minerals contained in the rocks, such as iron-titanium oxides and iron-sulphides. It does not seem to the present authors, therefore, the magnetic properties of so-called non-ferromagnetic minerals, such as silicates, which constitute over 95% of common rocks have ever attracted much attention of the investigators of rock-magnetism. In the present study, the magnetic susceptibility of some olivines, which are among the commonest rock-forming minerals, has been measured in order to clarify the paramagnetic nature of silicate minerals containing magnetic ions (Fe^{+2} in the case of olivines $x\mathrm{Fe_2SiO_4}\cdot(1-x)\mathrm{Mg_2SiO_4}$).

Among the rock-forming minerals, ionic crystals which are composed of the ions with complete electronic configurations like those of inert gas atoms ($^1S_0$) and covalent crystals in which the valence electrons are antiparallel in spin are diamagnetic, while those minerals containing ions with incomplete shell configurations as the transition elements are presumed to exhibit paramagnetic properties. Since olivines are the members of the solid solution between fayalite ($\mathrm{Fe_2SiO_4}$) and forsterite ($\mathrm{Mg_2SiO_4}$), in which the bonding between metallic ions and SiO_4 tetrahedrons is ionic and the bonding inside the tetrahedrons is covalent, the value of magnetic susceptibility is expected to vary with the ratio of forsterite to fayalite.

---

* Contribution from Division of Geomagnetism and Geoelectricity, Geophysical Institute, Tokyo University, Series II, No. 66

2. Samples Used and the Method of Measurement

The samples examined in the present study, rendered by Prof. H. Kuno, Geological Institute, Tokyo University, are listed in Table I. The chemical composition of them was determined either by chemical analysis or measurement of the refractive index.

After pulverized, each sample was fractioned by a Hallimond-type magnetic separator manufactured by Mitamura Co. Tokyo. Some results of the magnetic separation are illustrated in Fig. 1: the ordinate represents the amount of fractions yielded in traps A,B,C,D and E, which are in a decreasing order of the intensity of magnetism. These fractions will be called, in the following, the fraction A, fraction B, etc. Franction A, small in quantity, was always identified as magnetite through the measurement of the temperature variation of magnetization and by *X*-ray analysis. It was, moreover, observed that the fraction B could be sub-fractioned into the fraction A and the weaker fractions by further pulverization. Although these ferromagnetic impurities are small in quantity, they are the predominant factor in determining the apparent magnetic properties of the natural olivines, because the ferromagnetism of magnetite is stronger than the paramagnetism of olivines by a factor larger than 10^5*.

Table I. Olivine samples examined and their magnetic susceptibility at room temperature.

Locality	Source	$\frac{\text{Fayalite}\times 100}{\text{Fayalite}+\text{Forsterite}}$ in mol.	Paramagnetic susceptibility	
			specific (10^{-5} emu/gr)	molecular (10^{-3} emu/mol
Iizakamura, Hukusima Pref.	iron knebelite in pegmatite	98.4[1]	10.3	20.8
Huzi-Misima, (D) Sizuoka Pref,	olivine phenocrysts in basalt	35～29[2]	2.7	4.3
,, (E)	,,	34～31[2]	3.1	5.0
Mt. Muie, (C) Transvaal	dunite in Bushveld complex	33～30[2]	2.3	3.7
,, (D)	,,	34～29[2]	2.5	4.0
,, (E)	,,	32～29[2]	2.5	4.0
Isizumigahana, Hatizyô-zima Island	inclusion in anorthite crystals in andesite pumice	17.5[3]	2.4	3.6
Itinomegata, Akita Pref.	olivine-rich inclusion in basalt	10.6[4]	1.8	2.6
Miyako, (D) Iwate Pref.	forsterite in marble	4[2]	0.4	0.6
,, (E)	,,	4[2]	1.1	1.6

(C), (D), (E) mean the fractions separated by the magnetic separator.

[1]K. Omori and S. Hasegawa, Sci. Rep. Tôhoku Univ. ser. III, vol. IV, no. 1 (1951).

[2]Private communication from S. Aramaki, Geological Institute, Tokyo University.

[3]Private communication from N. Issiki, Geological Survey, Japan.

[4]C.S. Ross, M.D. Foster and A.T. Myers, Amer. Mineralogist, **39**, 693-737 (1954).

* Separation of minerals by magnetic separator such as Hallimond-type one is, thus, considered to be effected by rather the difference in the amount of ferromagnetic impurities than the difference in the intensity of inherent paramagnetism.

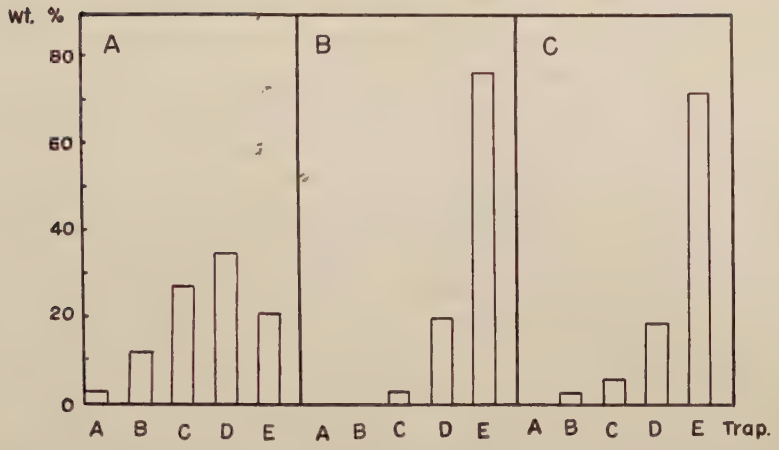

Fig. 1 Examples of magnetic separation by a Hallimond-type magnetic separator: A....olivine in dunite, Transvaal: B....olivine phenocrysts in basalt, Huzi-Misima: C....forsterite in marble, Miyako.

Consequently, we studied the magnetism of pure olivines after getting rid of the magnetite impurities as perfect as possible.

The magnetic measurements were all conducted by a sensitive quartz spring magnetic balance described elsewhere [1]. In spite of laborious removal of the magnetite impurities, even the weakest fraction of the olivines (fraction E) was found to contain a little amount of magnetite. In Fig. 2, *curve a* schematically shows the magnetization curve of a sample examined. The curve was interpreted as composed of the magnetization curve of paramagnetic olivine (*curve b*) and that of ferromagnetic impurity (*curve c*). Therefore, the paramagnetic susceptibiliy of olivine was obtained from the slope of the straight line part AB. In the actual process, the effect due to the imperfect saturation of the ferromagnetic part was also taken into account. On certain samples, the temperature dependence of the susceptibility was also measured and it was ascertained that the initial curved part of the magnetization curve disappeared at temperatures higher than the Curie point of magnetite.

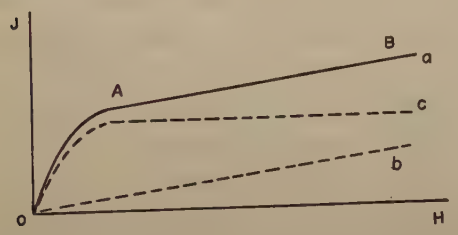

Fig. 2 Schematic representation of magnetization curve of olivine: *curve a*....curve actually measured: *curve b*....curve for purely paramagnetic olivine: *curve c*.... curve for ferromagnetic impurity.

3. The Results of Measurement

The molecular magnetic susceptibility at the room temperature of the samples measured by the above method is tabulated in Table I and plotted in Fig. 3 against the ratio of fayalite to forsterite. Some examples of magnetization curves measured are shown in Fig. 4, where the hollow circles represent the magnetization of the

fractions C,D and E of the olivine from dunite at Transvaal and the full circles are for the fraction E of the olivine from anorthite crystals in andesite pumice at Hatizyô-zima Island. In Fig. 4, it may be observed that the fractions C,D,E of the Transvaal sample

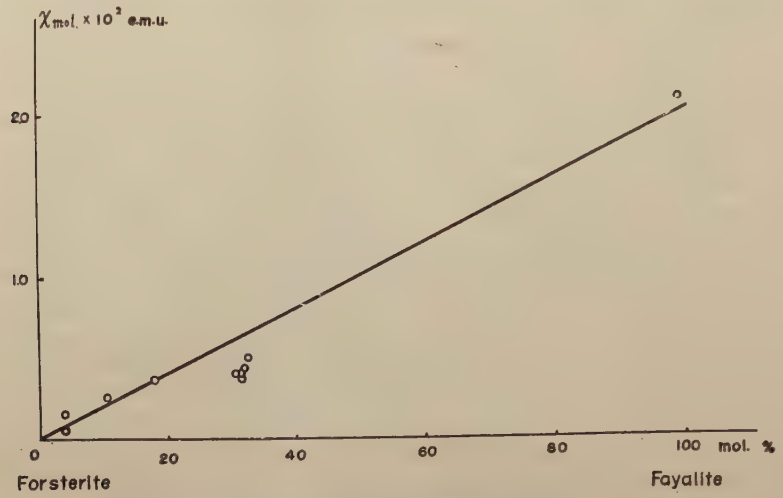

Fig. 3 Relation between the magnetic susceptibility of olivine and the fayalite content at room temperature.

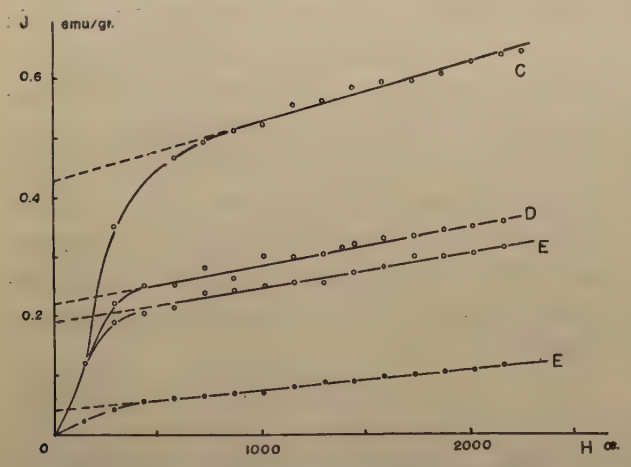

Fig. 4 Examples of observed magnetization curve of olivines at room temperature: full circles....fraction E of olivine extracted from anorthite crystals in andesite pumice, Hatizyô-zima Island: hollow circles....fractions C, D and E of olivine in dunite, Transvaal.

are nearly equal in paramagnetic susceptibility, whereas they differ in the amount of ferromagnetic impurity. This result seems to support the statement in the footnote in § 2.

From the results in Fig. 3, it may be stated that the magnetic susceptibility increases with content of fayalite nearly proportionally to the latter. As a first approximation, this relation can be expressed by the following empirical formula, at the room temperature:

$$\chi_{mol} = 2x \times 10^{-2} \ emu/mol, \qquad (1)$$

where x denoting the mol. percent of fayalite.

4. Discussion on the Results

Now, the magnetism of olivines is considered to consist of two parts, namely the paramagnetism originated from Fe^{+2} ions and the diamagnetism originated from all

the constituents. Therefore, the resultant magnetic susceptibility χ can be expressed as,

$$\chi = \chi_P + \chi_D, \tag{2}$$

where χ_P and χ_D representing the paramagnetic and diamagnetic susceptibilities. Although the contribution of diamagnetism in the present substance is not known, it may be presumed that we can neglect the second term in (2) to a good approximation.

The effective Bohr magneton number p_B of Fe^{+2} ion in crystal is known to be 5.1～5.55 when calculated from the Curie's law [2]. Using these values for the effective Bohr magneton number in the Curie's law, the magnetic susceptibility per gramme ion of Fe^{+2}, $\chi_{Fe^{+2}}$ is enumerated as,

$$\chi_{Fe^{+2}} = \frac{N_L \mu_B^2}{3kT} p_B^2 = \frac{3.23}{T} \sim \frac{3.82}{T}, \tag{3}$$

where N_L, μ_B, k and T are the Avogadro number, the Bohr magneton, the Boltzmann's constant and the absolute temperature respectively. If, further, we assume that the magnetic moment of Fe^{+2} ion is isolated from that of other Fe^{+2} ions in the olivine crystal, the molecular and the specific magnetic susceptibilities of fayalite (Fe_2SiO_4) at the room temperature become,

$$\begin{aligned} &\chi_{mol\ \ fayalite} = \chi_{Fe^{+2}} + \chi_{Fe^{+2}} = 2.2 \times 10^{-2} \sim 2.6 \times 10^{-2} emu/mol. \\ &\chi_{fayalite} = 11 \times 10^{-5} \sim 13 \times 10^{-5}\ emu/gr. \end{aligned} \tag{4}$$

As a result, the molecular magnetic susceptibility of any member of the solid solution $x Fe_2SiO_4 \cdot (1-x) Mg_2SiO_4$ at the room temperature can be expressed as,

$$\chi_{mol\ \ olivine} = 2.2x \times 10^{-2} \sim 2.6x \times 10^{-2}\ emu/mol. \tag{5}$$

Taking the experimental error introduced by the unavoidable presence of the ferromagnetic impurities into consideration, the agreement between the empirical formula (1) and the calculated one (5) seems to support the idea that the magnetic properties of olivine is attributable to the paramagnetism of Fe^{+2} ions isolatedly embedded in the crystal structure. If such agreement is to be expected to hold as a general rule, the paramagnetic susceptibility of various minerals will also be obtained by simple calculation of the following formula,

$$\chi_{mol} = \frac{N_L \mu_B^2}{3kT} \Sigma n_i p_{Bi}^2 = \frac{0.124}{T} \times \Sigma n_i p_{Bi}^2, \tag{6}$$

where the summation should be made for all the magnetic ions contained, and n_i and p_{Bi} denote the number of the i-th magnetic ions in a molecule and the effective Bohr magneton number of the same ions. For instance, the molecular paramagnetic susceptibility of orthopyroxenes ($x FeSiO_3 \cdot (1-x) MgSiO_3$), namely the solid solution between orthoferrosilite ($FeSiO_3$) and clinoenstatite ($MgSiO_3$) can be expected to be the half of the value in (5). Further examination on various rock-forming minerals containing magnetic ions will be effective in confirming the present result as a general rule.

Finally, the authors should like to express their sincere gratitude to Prof. H.

Kuno who kindly rendered them the useful samples and to Dr. S. Akimoto and Dr. S. Iida for valuable discussions.

References

[1] S. Akimoto, Journ. Geomag. Geoele., **6**, 1 (1954).

[2] E. Stoner, Magnetism and Matter, p. 312, Methuen, London, (1934).

LETTER TO THE EDITOR

Disturbances in the $F1$ and E Regions of the Ionosphere Associated with Geomagnetic Storms

It was pointed out by Berkner and Seaton [1] that the critical frequencies (f_0F1, f_0E) and the virtual heights (($h'F1$, $h'E$) of the $F1$ and E regions begin to vary at the same time when those in the $F2$ region do in the storm time. However, up to date the details of the variations in the $F1$ and E regions have been overlooked. One of the reasons may be that the variations in those regions at night cannot be known and the other that the deviations from the normal value are small compared with those in the $F2$ region. The purpose of this report is to show statistically the characteristics of the deviations in those regions.

(i) In low sunspot or geomagnetic activities, the deviations of f_0F1 and f_0E are small (especially the latter) and the amplitudes of them are often of the order of magnitude comparable with the error of the measurement. But with the increasing activity the amplitudes increase enough to admit as a disturbance. The disturbances in the $F1$ and E regions are classified in two types, the same as in the $F2$ distudance, positive and negative disturbances. The former is a disturbance in which the critical frequency of the region increases and the latter a disturbance in which it decrese. As shown in Figs. 2 and 3, the occurrence of the respective type of the disturbance depends on the season, latitude and geomagnetic or sunspot activities. The two types of the disturbance are shown in Fig. 1 for four stations. In that figure Δf_0F1 etc. represent deviative values from the respective normal values. Each variation is the mean of the variations on the first and second days for the moderate or severe disturbances during the period shown in the figure. From Fig. 1 it is found that the daily variation (only in daytime) of each type is similar to that in the $F2$ region. The deviation in the height seems to show an increase in the storm time. However, as $\Delta h'E$ (sometimes $\Delta h'F$) is considered to be the magnitude comparable with the error in the height measurement and a correction of the retardation of the wave through the E region is not made for $\Delta h'F1$, the increments of the height in two regions are doubtful.

(ii) In Fig. 2 the daily mean values ($\overline{\Delta f_0F1}$, $\overline{\Delta f_0E}$) of the Δf_0F1 and Δf_0E are plotted against the mean value ($\overline{\Delta f_0F2}$) of the $\Delta foF2$ during the hours when the Δf_0F1 and Δf_0E are taken. From Fig, 2 the following points are recognized.

(a) The positive correlation between the $\overline{\Delta f_0F1}$ or $\overline{\Delta f_0E}$ and $\overline{\Delta f_0F2}$ seems to be good. This correlation is better in high latitudes than in low and for $\overline{\Delta foF1}$ than for $\overline{\Delta f_0E}$.

(b) The amplitude of $\overline{\Delta f_0F1}$ and $\overline{\Delta f_0E}$ increases linearly in proportion to the amplitude of $\overline{\Delta foF2}$.

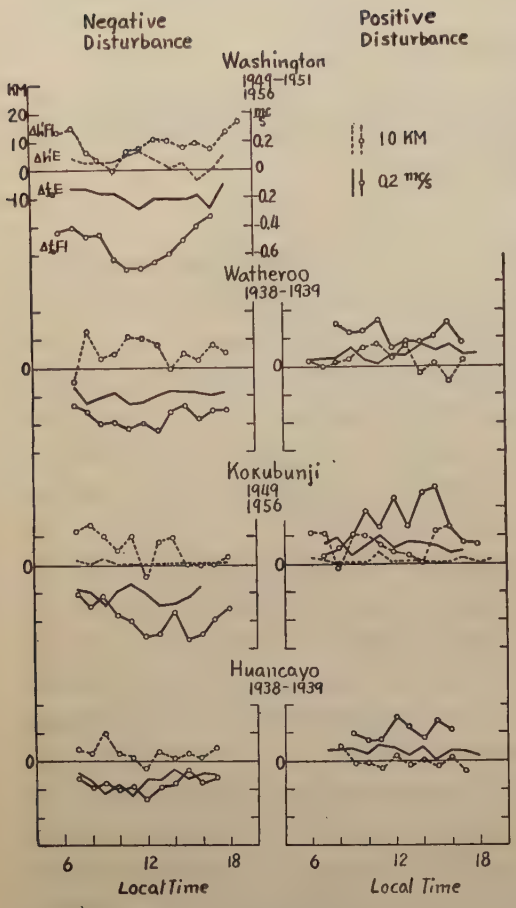

Fig. 1 Mean daily variations of Δf_0F1, Δf_0E, $\Delta h'F1$ and $\Delta h'E$ for moderate and severe disturbances during the period shown in the figure. Δf_0F1 etc. represent the deviative values from the respective normal values. The left-hand side shows the variation in the negative disturbance and the right-hand side in the positive disturbance.

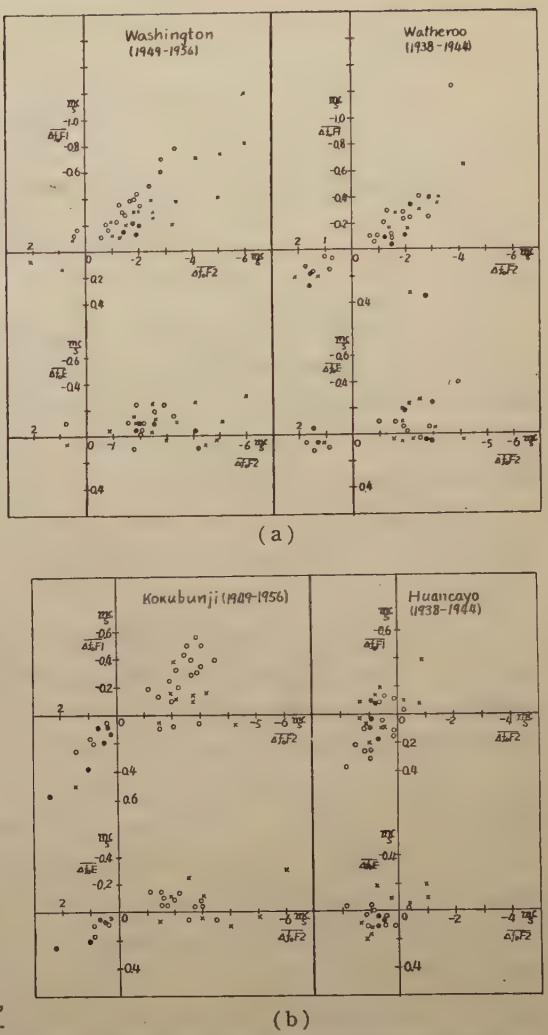

Fig. 2 Relation between $\overline{\Delta f_0F1}$ and $\overline{\Delta f_0E}$ in the disturbance occurred in four stations and the corresponding $\overline{\Delta f_0F2}$. $\overline{\Delta f_0F1}$ and $\overline{\Delta foE}$ represent the daily mean values of Δf_0F1 and Δf_0E and $\overline{\Delta f_0F2}$ the mean value of $\Delta foF2$ during the hours when f_0F1 and f_0E appear. The negative value represents the negative disturbance and the positive the positive disturbance. ° reperesents the value in summer, • winter and × equinox.

(c) In high latitudes $foF1$ and f_0E tends to decrease in the storm time (negative disturbance), in low latitudes (including the equator) they tend to increase (positive disturbance) and in middle latitudes they increase generally in winter and decrease in summer and equinox.

(iii) In Fig. 3 the values of $\overline{\Delta f_0F}$ and $\overline{\Delta f_0E}$ for three stations are plotted against respectively ΣKp (sum of the three hourly Kp indices of a day) and against the provisional sunspot number at Zurich in the month when the disturbance occurs. The

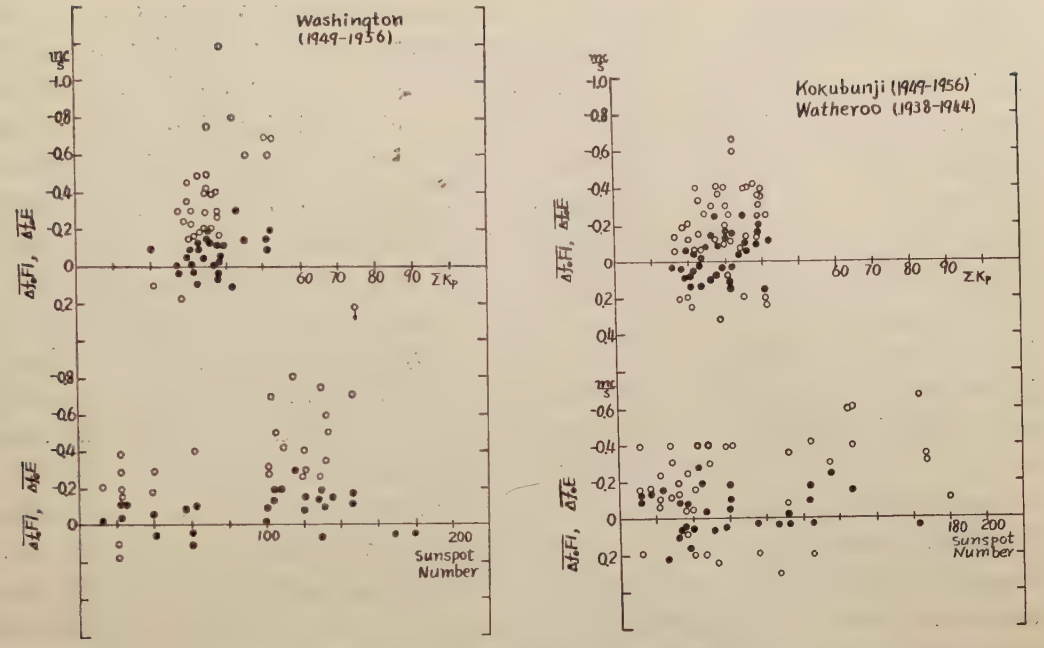

Fig. 3 Relation between $\overline{\Delta foF1}$ and $\overline{\Delta foE}$ and ΣKp (sum of three hourly Kp indices of a day) and the mean provisional sunspot number at Zurich in the month when the disturbance occurs. ° represents $\overline{f_0F1}$ and · $\overline{f_0E}$.

ordinate represents $\overline{\Delta f_0F1}$ and $\overline{\Delta f_0E}$ and the abscissa respectively ΣKp and sunspot number. From this figure the following points are recogniced.

(a) $\overline{\Delta f_0F1}$ and $\overline{\Delta foE}$ increase in proportin to both ΣKp and sunspot number.

(b) In middle latitudes the positive disturbance is easy to occur during the years of low sunspot or geomagnetic activities.

(**iv**) From the above results it is found that the daily variation and the latitudinal and seasonal changes of the types of Δf_0F1 and Δf_0E in the storm time show the analogous feaures to those of $\Delta foF2$. These facts lead to a consideration that the disturbances in the $F1$ and E regions are caused by the same mechanism as that in the case of the $F2$ distubance, and it seems to be suitable to take the electron drift theory as the cause of the $F1$ and E disturbances as well as the $F2$ disturbance [2], [3]. Again, we are forced to admit the above theory the best from a fact that the disturbances in the $F2$, $F1$ and E region begin simultaneously, because the other theories, for example, the thermal expansion, recombination, are difficult to explain the above fact.

From the view point of the drift theory we explain the statistical results shown above as follows (the same explanation is described in the case of the $F2$ disturbance [4], [5], so that the brief description is given here). In the storm time the electric field originated in the polar region spread over the world and the vertical drift of the electron takes place due to this electric field and the geomagnetic. This velocity v_d is dedueed from the geomagnetic disturbance-daily variation. On the other hand, the vertical drift with the velocity v_q is present on a quiet day. The velocity is derived

from the *Sq* geomagnetic variation. On the disturbed day a vertical drift of the electron with the velocity (v_d+v_q) occurs. The maximum electron density on a quiet day is, on account of the presence of the vertical drift with the velocity v_q, smaller than that in the static region. Therefore if the daily variation of v_d has the same phase as that of v_q, the reduction is promoted on the disturbed day. This is a negative disturbance. On the contrary, if the phase of the velocity v_d is different by about 180° from that of v_q the (v_q+v_d) becomes samller than v_q and the maximum electron density increases, because the region is analogous to the no-movement region. This is the positive disturbance. The former case is easy to occur in high latitudes and the latter in low latitudes (or in the equator), for the phase of v_q differs depending on the latitude in spite of the invariability of the phase of v_d. In middle latitudes the relation between the phases of v_d and v_q in summer and equinox is analogous to that in high latitudes and the relation in winter is analogous to that in low latitudes. Therefore the latitudinal and seasonal changes of the type of the disturbance appear as shown in Fig. 2. That the lower the region, the smaller the deviation is ascribed to the fact that the drift in lower region (much the same as in the upper region) becomes less effective due to the increase of the production and the decay of the electron. Martyn introduced the height gradient of the drift velocity in his rough estimation of the deviation in the $F2$ disturbance. Even if such a gradient exists, it is necessary that the gradients in the $F2$, $F1$ and E region are the same, inferring from the proportionality of the deviations as shown in Fig. 2. Actually, the necessary gradients of the drift velocity due to the electric field are probably difficult to occur in the $F1$ and E regions and also we do not need the gradient in the explanation of the $F2$ disturbance. Next, in the high sunspot activity the f_0F1 and f_0E themselves (and also f_0F2) are large compared with those in the low activity, so that the Δf_0F1 and Δf_0E (Δf_0F2) are larger, even if the deviation of the electron density is the same percentage. In the high geomagnetic activity (which is easy to occur in the high sunspot activity) the v_d becomes larger compared with that in the low activity (that is, $(v_d+v_q)\simeq v_d$). Then the variation (negative, or to the negative) is promoted since the drift with the veloety v_d gives the effect of a reduction of the electron density in daytime, and somtimes removes the latitudinal and seasonal dependency.

References

[1] L.V. Berkner and S.L. Seaton, Terr. Mag., **45**, 393 (1940)
[2] D.F. Martyn, Nature, **171**, 14 (1953); Proc, Roy. Soc., A, **218**, 1 (1953)
[3] K. Maeda, Rep. Iono. Res. Japan, **7**, 81 (1953)
[4] T. Sato, J. Geomag. Geoele., **8**, 129 (1956)
[5] T. Sato, J. Geomag. Geoele., **9**, 1 (1957) (In this issue.)

by Teruo Sato
Geophysical Institute, Kyoto Universjty

JOURNAL
OF
GEOMAGNETISM
AND
GEOELECTRICITY

VOL. VIII

1956

SOCIETY

OF

TERRESTRIAL MAGNETISM AND ELECTRICITY

OF

JAPAN

KYOTO

JOURNAL OF GEOMAGNETISM AND GEOELECTRICITY

TABLE OF CONTENTS

Vol. VIII, No. 1, 1956

Vol. VIII, No. 2, 1956

Vol. VIII, No. 3, 1956

Vol. VIII, No. 4, 1956

JOURNAL OF GEOMAGNETISM AND GEOELECTRICITY

Vol. VIII, 1956

INDEX OF AUTHORS

Meeting of the Society of Terrestrial Magnetism and Electricity:

The 20th General Meeting was held at the Kyoto University on October 16-18, 1956.

Number of the Reports read at the Meeting:

Rock Magnetism, 8; Atmospheric Electricity, 4; Radio Meteorology, 6; Geomagnetism and Earth Current, 13; Ionosphere, 13; Cosmic Rays, 8.

Tanakadate Prize was awarded for the following excellent worker:

The 20th, Mr. T. Sato;

Investigations on Disturbances in the Ionospheric $F2$ Region Associated with Geomagnetic Storms Based on the Ionization Drift Theory.

The 21th General Meeting was held at the Tokyo University on May 10–12, 1957.

Number of the Reports read at the Meeting:

Geomagnetism, 18; Ionosphere, 11; Night Airglow, 3; Cosmic Rays, 6; Rock Magnetism, 9; Atomospheric Electricity and Radio Meteorology, 12; Special Report on Antarctic Research Expedition, 10.

Tanakadate Prize was awarded for the following excellent worker:

The 21th, Mr. H. Ishikawa;

On waveforms of atmospherics of short distances and lightning discharges.

昭和32年7月20日　印刷
昭和32年7月25日　發行
第9卷　第1號

編輯兼發行者　日本地球電氣磁氣學會
代表者　長谷川万吉

印刷者　京都市南区上鳥羽唐戸町63
田中幾治郎

賣捌所　丸善株式會社京都支店
丸善株式會社 東京・大阪・名古屋・仙台・福岡

JOURNAL OF GEOMAGNETISM AND GEOELECTRICITY

Vol. IX No. 1

1957

CONTENTS